Metamaterials With Analogous Electromagnetically Induced Transparency and Related Sensor Designs—A Review

Zhixia Xu, *Member, IEEE*, Yi Wang, Siyuan Liu, *Graduate Student Member, IEEE*, Jitong Ma, Shaojun Fang, and Haotian Wu

***Abstract*—Electromagnetically induced transparency (EIT) originates from quantum physics, where a narrow transparent peak appears in the opaque band due to the destructive interference between quantum states of atoms and molecules. Similar phenomena can be realized based on strong-coupling resonators with a similar spectrum of transmission peaks and abrupt dispersion variations. These classical systems, ranging from elastic to optical, are named analogs of EIT. The sharp resonant peaks with high-quality factors in the spectrum exhibit powerful potentials in sensors with ultrahigh sensitivity. In order to better understand the development history of EIT-like metamaterials and their specific applications in the field of sensors, this article makes a brief review of the EIT-like phenomenon in metamaterials. First, we conduct the universal mathematical formulation based on the coupling oscillator model. Then, we classify specific metamaterial designs and practical applications of EIT-like devices in acoustic, electromagnetic, and optical waves, respectively. We also summarize the recent technologies of dynamic modulations of EIT-like metamaterials and discuss future research directions.**

***Index Terms*—Electromagnetically induced transparency (EIT), metamaterials, resonators, spectrum, strong coupling.**

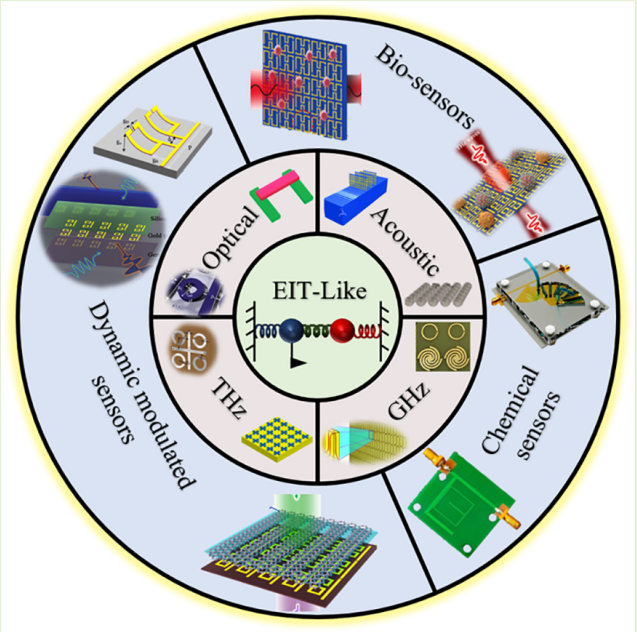

Manuscript received 16 January 2023; revised 23 February 2023; accepted 23 February 2023. Date of publication 3 March 2023; date of current version 31 March 2023. This work was supported in part by the Dalian Youth Science and Technology Star Project under Grant 2022RQ034, in part by the State Key Laboratory of Millimeter Waves under Grant K202202, in part by the National Natural Science Foundation of China under Grant 62101090, and in part by the China Postdoctoral Science Foundation under Grant 2021M700656. The associate editor coordinating the review of this article and approving it for publication was Prof. Carlos Marques. *(Corresponding authors: Zhixia Xu; Haotian Wu.)*

Zhixia Xu is with the School of Information Science and Technology, Dalian Maritime University, Dalian 116026, China, and also with the State Key Laboratory of Millimeter Waves, Southeast University, Nanjing 210096, China (e-mail: zhixiaxu@dlmu.edu.cn).

Yi Wang, Jitong Ma, and Shaojun Fang are with the School of Information Science and Technology, Dalian Maritime University, Dalian 116026, China (e-mail: majitong@dlmu.edu.cn).

Siyuan Liu is with the State Key Laboratory of Millimeter Waves, Southeast University, Nanjing 210096, China (e-mail: m18951892170@163.com).

Haotian Wu is with the School of Electrical and Electronic Engineering, Nanyang Technological University, Singapore 639798 (e-mail: haotian.wu@ntu.edu.sg).

Digital Object Identifier 10.1109/JSEN.2023.3249743

I. Introduction

THE concept of electromagnetically induced transparency (EIT) originated from quantum physics [1], [2], [3], [4], where the destructive interference between different atomic excitation paths causes a narrow and sharp transparent peak in the absorption background [5], [6], [7], [8]. Along with the sharp transmission window, the dispersion changes abruptly [9], [10], [11]. Quantum EIT experiments require low temperature and laser source [12], [13]. Associated with the EIT is the dramatic modification of the refractive properties, which can be revealed by slow group velocities at the transparent peak [14]. In prior works, the light slows down to a group velocity of about 17 m/s [15], and even the storage of light is possible [16], [17]. EIT systems have also been studied in atomic vapors. Santra et al. [18] proposed an optical clock scheme by establishing coherent coupling between the ground and the excited states, eliminating the Doppler effects. The clock accuracy reaches better than 2×10^{-17}. In 2007, Mohapatra et al. [19] demonstrated coherent optical detection

This work is licensed under a Creative Commons Attribution 4.0 License. For more information, see https://creativecommons.org/licenses/by/4.0/

of highly excited EIT states, which shows that the EIT spectra allow direct optical detection of electric field transients in the gas phase. Buth et al. [20] studied EIT based on X-rays, paving the development of ultrafast X-ray sources. In recent years, Liu et al. [21] used Rydberg atoms as microwave antennas and modems to detect phase-modulated multifrequency microwave fields through the EIT effect.

In recent years, the exploration of the analog of EIT in classical systems has been developed based on coupled resonances [22], [23], which can be explained according to the bright-dark- and bright-bright-mode theories [24], [25], [26], [27]. A traditional EIT-like system consists of at least two resonators. The bright-mode resonator has a wide bandwidth with a low quality (Q) value, and it can be directly excited by the external source. The dark-mode resonator has a narrow bandwidth with a high Q value. The dark-mode resonator cannot be directly excited by the external source, but it is strongly coupled with the bright mode due to the overlapping resonant frequencies. The strong coupling system can generate a very sharp peak in the spectrum, accompanied by abrupt phase changes [26], [27]. Recent researches show the possible realization of multiple EIT-like transmissions [30], [31], [32] and the EIT-like behavior in a single resonator [33], [34]. Due to the similarity of the spectrum of the coupling system and that of the quantum EIT behavior, we can denote these classical systems as EIT-like systems. EIT-like devices have been widely used in the field of sensors [35], [36], [37], [38], [39], [40], such as chemical, biomedical, and metal detection [41]. EIT-like sensors have been developed for the measurement of complex permittivity of liquids [32], [42] and the detection of cancer cells [43], [44]. It is worth noting that the THz spectral domain is of particular significance for sensing applications, thanks to the unique "fingerprint signature" of many analytes found in nature. THz sensors are widely utilized due to their numerous advantages, such as high sensitivity and noninvasiveness. EIT-like sensors, which are extremely sensitive to the external environment, are even more sensitive than non-EIT-like sensors. In addition to sensing applications, EIT-like devices can also be used for slow-light devices [45], [46], [47], [48], optical modulators [49], [50], absorbers [51], [52], [53], [54], optical switches [55], and optical memories [56], [57].

In this article, we briefly review the development of EIT-like systems. Section I is the introduction. In Section II, we formulate the theoretical models, including the atomic model in the quantum field, and compare it with coupling-oscillator models in the classical regime. We also conduct a parameter analysis to show the change in the spectrum. Section III reviews the EIT-like metamaterial designs from acoustic regime to electromagnetic waves. In Section IV, various EIT-like metamaterial sensors are reviewed. Section V reviews recent tunable EIT-like metamaterials based on various modulation technologies, and we look at the field's future development in Section VI.

II. Theoretical Models

A. Atomic Energy Level Model

1) Three-Level Λ-Type Scheme: As shown in Fig. 1(a), the three-level Λ-type scheme can be explained as interactions among three energy levels and two laser beams [1], [58], [59]. States 1 and 2 represent two ground states, and state 0 represents the excited state. The laser used to drive the atomic transition between quantum states 1 and 0 is called the pumping laser of frequency ω_p, and the laser that drives the atomic transition between quantum states 0 and 2 is called the probing laser of frequency ω_b. Without the action of ω_p, it is possible to observe a standard absorption profile. When ω_p is added, a narrow induced EIT peak appears in the absorption profile. The existence of this effect mainly depends on the intensity of ω_p.

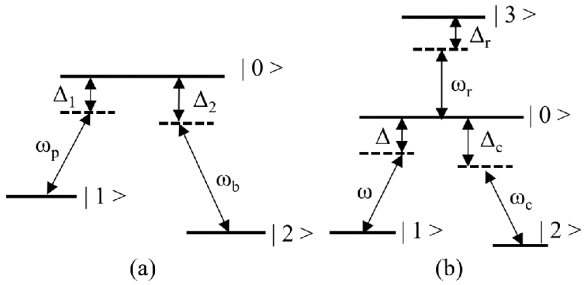

Fig. 1. Quantum atomic models. (a) Three-level Λ-type EIT scheme. (b) Four-level invert-Y-type scheme.

2) Four-Level Invert-Y-Type Scheme: Multiple EIT peaks can be used for the bifurcation of multichannel quantum information. By manipulating the group velocity of the individual channels, the release of stored information from multiple channels can be individually controlled. Therefore, double-EIT technology is essential in quantum information processing and computing [60]. The three-level Λ-type scheme can generate only one EIT peak. Furthermore, the double EIT transmission peak can be expressed by the atomic four-level invert-Y-type scheme [61], [62], as shown in Fig. 1(b) [60]. The transition between quantum states 0 and 1 depends on the probing laser of frequency ω. A coupling laser of frequency ω_c induces the transition between quantum states 0 and 2, and state 0 can be transferred to the higher order state 3 by a strong pumping laser of frequency ω_r. Atomic transitions of $0\leftrightarrow1$, $0\leftrightarrow2$, and $0\leftrightarrow3$ are allowed. When ω_c and ω_r coexist, double EIT peaks can be observed.

B. Classical Coupling-Oscillator Models

Originating from the quantum EIT phenomenon, various analogous EIT systems can be realized in the classical region. The coupling-oscillator model can provide universal explanations of high-Q modes related to EIT-like coupling, which is meaningful for sensor designs. In this review, the author starts from the double-oscillator model and extends the exploration to the multioscillator model to summarize a general analytical method for classical EIT-like systems.

1) Bright-Dark-Mode Theory: Bright modes represent resonant modes that can be directly excited by external incident waves, which usually have broadband absorption spectra and low Q values. The dark mode (DM) cannot be directly excited by an external source but can be excited by coupling resonance with the bright mode. Compared with the bright mode, the DM has the characteristics of narrowband and high Q value.

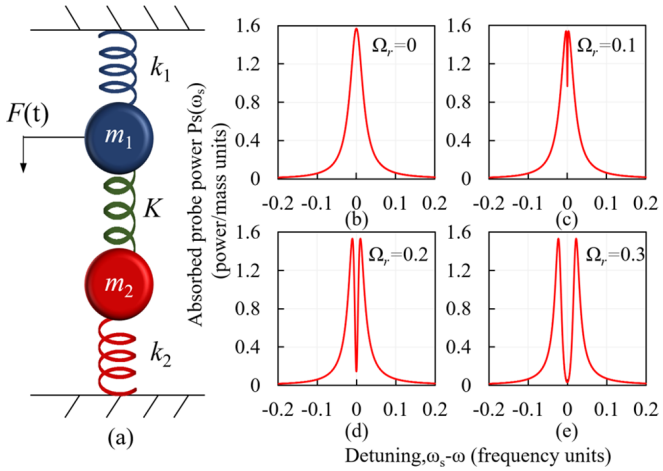

Fig. 2. Double-oscillator Model. (a) Configuration. The absorption spectrum of the particle 1. The values of coupling strength Ω_r are (b) $\Omega_r = 0$, (c) $\Omega_r = 0.1$, (d) $\Omega_r = 0.2$, and (e) $\Omega_r = 0.3$ in frequency units.

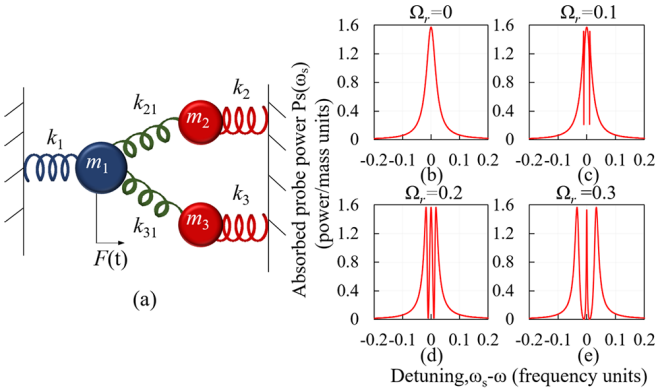

Fig. 3. Triple-oscillator model. (a) Configuration. The absorption spectrum of the particle 1. The values of Ω_r are (b) $\Omega_r = 0$, (c) $\Omega_r = 0.1$, (d) $\Omega_r = 0.2$, and (e) $\Omega_r = 0.3$ in frequency units.

In the theory of EIT, the existence of the transparent peak is due to the interference effect between the bright mode and the DM. We can also realize the analog of EIT in classical-resonance models, and related EIT-like modes with high Q are applicable in various devices. EIT-like structures are usually based on two coupling methods: bright-dark-mode coupling [63], [64], [65], [66] and bright-bright-mode coupling [67], [68]. Both two methods require the overlapping of center frequencies of different resonant modes. We further analyze the classical coupling-oscillator model to make an explanation. Among them, the springs connected between different particles represent the interference between different modes.

2) Double-Oscillator Model: Fig. 2(a) shows the classical double-oscillator model [69], [70], [71], [72], which consists of two particles with a certain mass and three springs with fixed spring constants. The masses of the particles are m_1 and m_2. The springs with constants k_1 and k_2 are fixed on the wall, and the spring with constant K connects the two particles. The external force $F(t)$ is put on bright-mode particle 1. Dark-mode particle 2 is not subjected to external force during the movement and only receives the force of the two springs connected to itself. We set $k_1 = k_2 = k$, $m_1 = m_2 = m$, and the particle's eigen-oscillation frequency $\omega_1 = \omega_2 = \omega$. The respective displacements of particles 1 and 2 are $x_1(t)$ and $x_2(t)$. The damping is denoted by γ_1 and γ_2, and the coupling strength $\Omega_r = (K/m)^{1/2}$. The displacement equation of the system can be expressed as

$$\begin{cases} \ddot{x}_1(t) + \gamma_1\dot{x}_1(t) + \omega^2 x_1(t) - \Omega_r^2 x_2(t) = \dfrac{F}{m}e^{-i\omega_s t} \\ \ddot{x}_2(t) + \gamma_2\dot{x}_2(t) + \omega^2 x_2(t) - \Omega_r^2 x_1(t) = 0. \end{cases} \tag{1}$$

We solve the specific expression for $x_1(t)$

$$x_1(t) = \frac{(\omega^2 - \omega_s^2 - i\gamma_2\omega_s)Fe^{-i\omega_s t}}{m\left[\left(\omega^2 - \omega_s^2 - i\gamma_1\omega_s\right)\left(\omega^2 - \omega_s^2 - i\gamma_2\omega_s\right) - \Omega_r^4\right]}. \tag{2}$$

The absorbed power of particle 1 in one period is expressed as

$$P_s(\omega_s) = -\frac{2\pi i F^2\omega_s(\omega^2 - \omega_s^2 - i\gamma_2\omega_s)}{m\left[\left(\omega^2 - \omega_s^2 - i\gamma_1\omega_s\right)\left(\omega^2 - \omega_s^2 - i\gamma_2\omega_s\right) - \Omega_r^4\right]}. \tag{3}$$

According to (3), we draw the variation curve of the absorbed power curve of particle 1 with the coupling strength Ω_r in Fig. 2(b)–(e). The values of each parameter are $\omega = 2$, $\gamma_1 = 4 \times 10^{-2}$, $\gamma_2 = 1 \times 10^{-3}$, $F = 0.1$ N, and $m = 1$ kg. When there is a coupling between two particles, a narrow-band appears in the absorption power spectrum of particle 1. As the coupling strength Ω_r increases, the depression becomes more evident, which is caused by the destructive interference between the two particles due to the strong coupling interaction.

3) Triple-Oscillator Model: With the increase in the number of coupled oscillators, the number of EIT-like sharp resonant modes increases [60]. The mechanical configuration is shown in Fig. 3(a). In this model, particle 1 is affected by the simple harmonic force $F(t)$; the other two particles are used to represent the DMs, and their masses are m_2 and m_3. All three particles are connected by using springs with constants of k_1, k_2, k_3, k_{21}, and k_{31}. Assuming that the displacement of the three particles is $x_i(t)$, their respective damping coefficients are γ_i, and the mass of the three particles $m_1 = m_2 = m_3 = m$, $k_{21} = k_{31} = K$, $\Omega_r = (K/m)^{1/2}$, and $\omega_i = (k_i/m)^{1/2}$, the displacement equation of the system at this time is

$$\begin{cases} \ddot{x}_1(t) + \gamma_1\dot{x}_1(t) + \omega_1^2 x_1(t) - \Omega_r^2 x_2(t) - \Omega_r^2 x_3(t) = \dfrac{F}{m}e^{-i\omega_s t} \\ \ddot{x}_2(t) + \gamma_2\dot{x}_2(t) + \omega_2^2 x_2(t) - \Omega_r^2 x_1(t) = 0 \\ \ddot{x}_3(t) + \gamma_3\dot{x}_3(t) + \omega_3^2 x_3(t) - \Omega_r^2 x_1(t) = 0. \end{cases} \tag{4}$$

The displacement equation of particle 1 is deduced as

$$x_1(t) = \frac{Fe^{-i\omega_s t}}{m\left[\left(\omega_1^2 - \omega_s^2 - i\gamma_1\omega_s\right) - \frac{\Omega_r^4}{\omega_2^2 - \omega_s^2 - i\gamma_2\omega_s} - \frac{\Omega_r^4}{\omega_3^2 - \omega_s^2 - i\gamma_3\omega_s}\right]}. \tag{5}$$

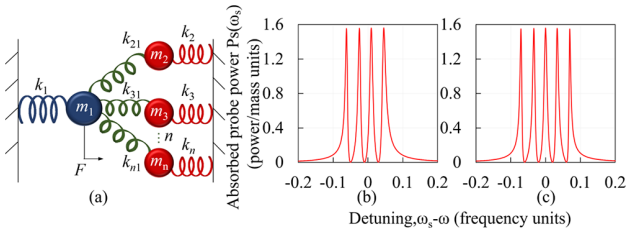

Fig. 4. Higher order oscillator model. (a) Configuration. The absorbed spectrum of particle 1 of (b) fourth and (c) models.

Therefore, the absorbed power in one period is calculated as

$$P_s(\omega_s) = \frac{-2\pi i F^2 \omega_s}{m\left[\left(\omega_1^2-\omega_s^2-i\gamma_1\omega_s\right)-\frac{\Omega_r^4}{\omega_2^2-\omega_s^2-i\gamma_2\omega_s}-\frac{\Omega_r^4}{\omega_3^2-\omega_s^2-i\gamma_3\omega_s}\right]}. \tag{6}$$

According to (4), we draw the relationship between the absorbed power of particle 1 and the coupling strength in Fig. 3(b)–(e). The values of each parameter $\omega_1 = 2$, $\omega_2 = 1.99$, $\omega_3 = 2.01$, $\gamma_1 = 4\times10^{-2}$, $\gamma_2 = \gamma_3 = 1\times10^{-4}$, $F = 0.1$ N, and $m = 1$ kg because, due to the different self-resonance frequencies of the two particles, there are two narrow dips in the absorption spectrum, corresponding to two transparent transmission peaks in the transmission spectrum.

4) Higher Order Oscillators' Model: We further extend to higher order oscillators and derive the general solutions. The higher order model is shown in Fig. 4(a), where the mass of particle i is m_i, the corresponding damping coefficient is γ_i, the spring constant connected is k_i, the self-resonant frequency $\omega_i = (k_i/m_i)^{1/2}$, and the displacement of the motion is $x_i(t)$. Assume that the constant of the spring connected between particles m and n is k_{mn}. Particle 1 is driven by the force $F(t)$, and other particles are not affected by external driving forces. The displacement equation of the whole mechanical vibrator system is

$$\begin{cases} \ddot{x}_1(t)+\gamma_1\dot{x}_1(t)+\omega_1^2x_1(t)-\sum_{i=2}^{n}\frac{k_{i1}}{m_1}x_i(t)=\frac{F}{m_1}e^{-i\omega_s t} \\ \ddot{x}_2(t)+\gamma_2\dot{x}_2(t)+\omega_2^2x_2(t)-\frac{k_{21}}{m_2}x_1(t)=0 \\ \cdots \\ \ddot{x}_i(t)+\gamma_i\dot{x}_i(t)+\omega_i^2x_i(t)-\frac{k_{i1}}{m_i}x_1(t)=0. \end{cases} \tag{7}$$

Assume that $\Omega_{ij}^4 = k_{ij}^2/m_i m_j$; we can deduce $x_1(t)$ as

$$x_1(t) = \frac{Fe^{-i\omega_s t}}{m_1\left[\left(\omega_1^2-\omega_s^2-i\gamma_1\omega_s\right)-\sum_{i=2}^{n}\frac{\Omega_{i1}^4}{\omega_i^2-\omega_s^2-i\gamma_i\omega_s}\right]}. \tag{8}$$

Therefore, the absorbed power of particle 1 in one period is

$$P_s(\omega_s) = -\frac{2\pi i F^2\omega_s}{m_1\left[\left(\omega_1^2-\omega_s^2-i\gamma_1\omega_s\right)-\sum_{i=2}^{n}\frac{\Omega_{i1}^4}{\omega_i^2-\omega_s^2-i\gamma_i\omega_s}\right]}. \tag{9}$$

This result is universal. When $n = 2$ or 3, it corresponds to (3) and (6), respectively. In order to further verify the correctness of (9), we describe the absorption spectrum in the four- and five-oscillator models, as shown in Fig. 4(b) and (c), respectively. In the four-oscillator models, parameters are $\omega_1 = 2$, $\omega_2 = 1.95$, $\omega_3 = 1.99$, $\omega_4 = 2.03$, $\gamma_1 = 4\times10^{-2}$, $\gamma_2 = \gamma_3 = \gamma_3 = 1\times10^{-4}$, $F = 0.1$ N, $m = 1$ kg, and $\Omega_r = 0.3$. In the five-oscillator models, parameters are $\omega_1 = 2$, $\omega_2 = 1.94$, $\omega_3 = 1.98$, $\omega_4 = 2.02$, $\omega_5 = 2.06$, $\gamma_1 = 4\times10^{-2}$, $\gamma_2 = \gamma_3 = \gamma_3 = \gamma_4 = 1\times10^{-4}$, $F = 0.1$ N, $m = 1$ kg, and $\Omega_r = 0.3$. When there are n particles, $(n-1)$ absorptive dips (transparent peaks) appear.

III. EIT-Like Metamaterial Designs

A. Analogous EIT in Acoustic Bands

The concept of acoustically induced transparency (AIT) metamaterials can be traced back to 2008, Boudouti et al. [73] proposed an acoustic filter consisting of two sites on an infinite slender tube, achieving Fano-like resonance with inducing transparency. Since then, various AIT metamaterials have been proposed. Amin et al. [74] designed and fabricated an AIT metasurface that produced Fano resonance. The structure is shown in Fig. 5(a), where each unit cell contains a pair of concentric pipes made of rigid acoustic material. In this structure, the AIT is generated by the destructive interference of two strongly coupled but detuned modes, as shown in Fig. 5(b). In 2016, Wang et al. [75] designed and fabricated a similar AIT device, as shown in Fig. 5(c). The structure is a planar periodic subwavelength element array [75]. The structure is composed of a pair of concentric spherical shells. The resonant frequency of the entire periodic structure depends on the size of the cavity and the opening angles of the spherical shell. In the single-cavity excitation state, the acoustic energy is confined in the spherical shell, and the inserted concentric spherical shell can further induce an AIT peak, as shown in Fig. 5(d). Besides various arrays to achieve AIT, the connection between phononic pillars and surface acoustic wave (SAW) is also explored. In 2018, Oudich et al. [76] developed a multilayered phononic pillars structure composed of Si and polymethylmethacrylate (PMMA), and placed it on the surface of the Si substrate to realize the mode coupling between SAW and phononic pillars. When there is no defect in the multilayered phononic pillars, the energy of SAW is confined to the surface of the phononic pillars and the Si substrate, resulting in attenuation of the SAW amplitude in a relatively wide frequency band. When defects are introduced into the multilayered phononic pillars, and the pillars are arranged periodically, as shown in Fig. 5(e), well-confined cavity modes can be created, which can couple with localized modes in the bottom of the pillar in contact with the substrate. The interaction can give rise to Fano-like resonance behavior and an acoustic analog of EIT for SAW. Due to the small amount of energy leakage and high transmission efficiency, it provides a new technical route for the design of high-performance sensing devices based on SAW.

B. Analogous EIT in GHz Bands

The EIT-like metamaterial was first realized in 2008, when Papasimakis et al. [77] designed a fish-scale double-layer

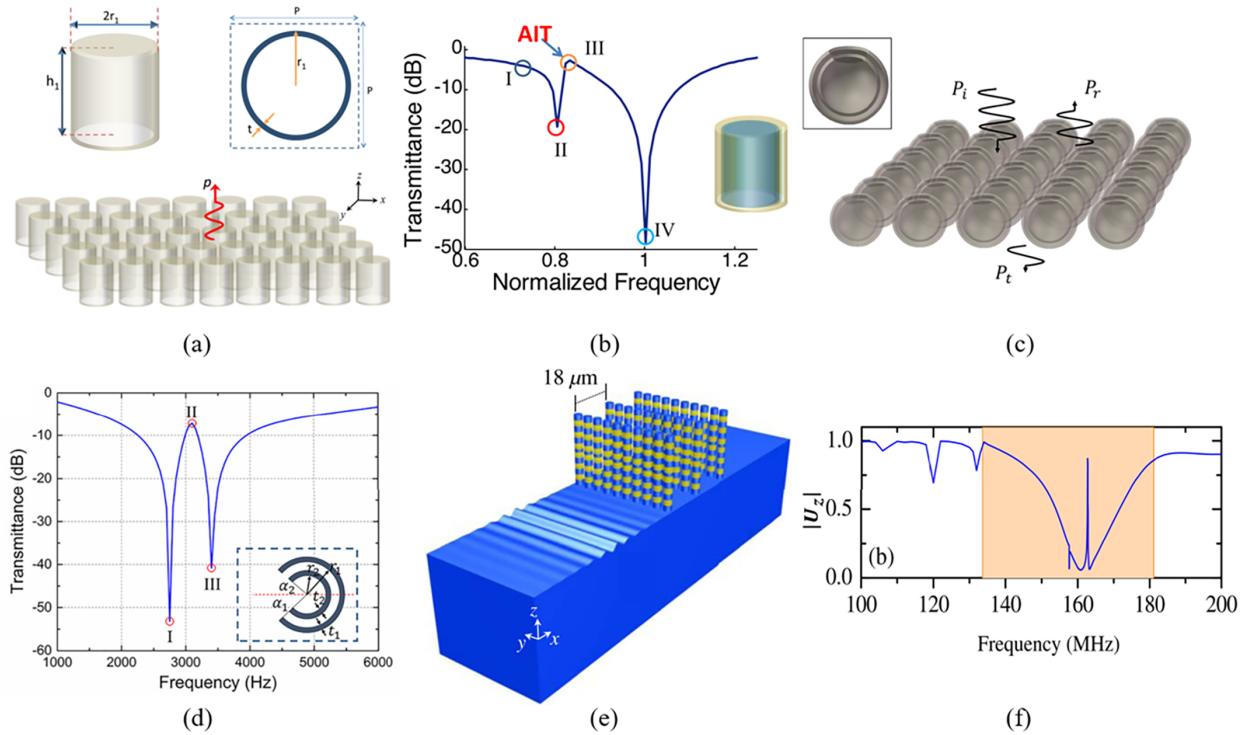

Fig. 5. AIT metamaterials. (a) Hollow cylindrical pipe and (b) its transmission spectrum [74]. (c) Array of the sphere and (d) its transmission spectrum [75]. (e) SAW transmission through rows of pillars and (f) its transmission spectrum [76].

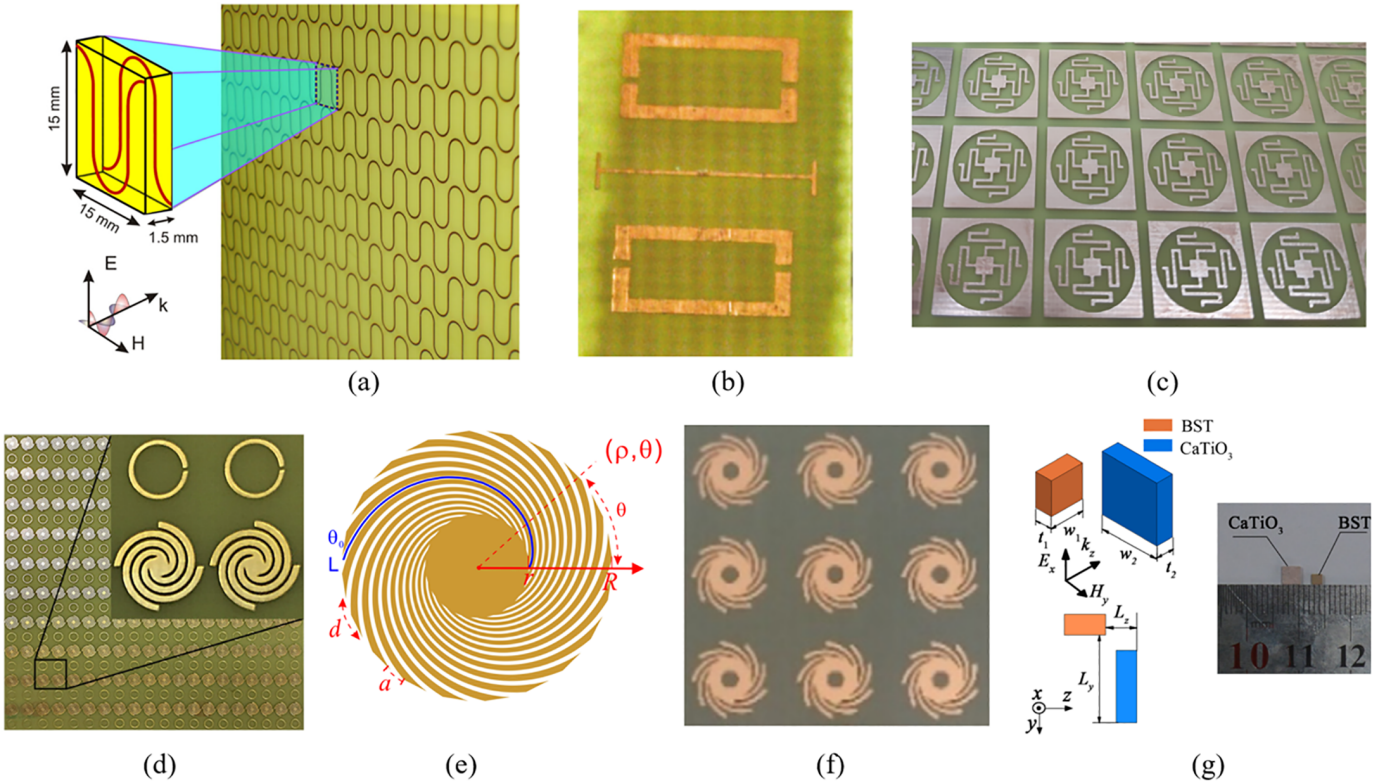

Fig. 6. Metallic EIT-like metasurfaces. (a) Fish-scale metasurface [77]. (b) EIT-Like metamaterial without breaking the symmetry [78]. (c) Ring and zigzag spiral metasurface [67]. EIT-like metasurfaces based on spoof LSP. (d) Magnetic spoof LSP metasurface [83]. (e) Single spiral spoof LSP metasurface [34]. (f) Logarithmic spiral spoof LSP metasurface [33]. (g) All-dielectric EIT-like metamaterials composed of BST and $CaTiO_3$ [88].

metasurface with a sharp transmission peak around 5.5 GHz, as shown in Fig. 6(a). Bright-dark mode coupling is the mainly used scheme for metallic EIT-like metamaterials. Zhang et al. [78] used two mirrored split-ring resonators (SRRs) and cutting wire (CW) as the dark and bright modes, respectively. The structure is shown in Fig. 6(b). The research

group realized the EIT-like effect without breaking the structural symmetry, and the two mirrored SRRs can suppress the magnetic dipole moment and increase the Q factor of the DM. The bright-bright mode can also be used to realize an EIT-like phenomenon. Tung et al. [67] proposed a polarization-insensitive periodic structure composed of the ring and zigzag spiral resonators, as shown in Fig. 6(c). Both ring resonators and zigzag spiral resonators can be excited by incident waves with different polarizations, and both of them resonate at the same frequency. When they are put together, a transparent window appears with a transmission peak. Since the structure is centrosymmetric, there is no shift in the transmission spectrum for different polarized incident waves.

Compared to traditional resonant structures, spoof localized surface plasmons (LSPs) contain more fruitful high Q modes and can achieve miniaturization [79], [80], [81], [82]. Some typical EIT-like metasurfaces based on spoof LSPs are shown in Fig. 6(d)–(f). In 2019, Xu et al. [83] proposed an analog of EIT based on bright-dark mode coupling between SRRs and spoof magnetic LSPs, as shown in Fig. 6(d). Only the SRRs can be externally excited, interacting with the neighboring dark spoof magnetic LSPs by near-field coupling. The conventional spoof LSP structure can achieve one transmission peak and generate multiple EIT-like peaks. Recently, researchers also found that only one structure can realize the EIT-like effect. Liu et al. [33] and Wu et al. [34] report the theoretical and experimental designs, respectively, as shown in Fig. 6(e) and (f). The electric and magnetic dipole modes in the carefully designed spiral spoof LSP overlap in a very narrow frequency band. The electric dipole is regarded as a bright mode, and the magnetic dipole is regarded as a DM.

Although metallic structures perform well in low-frequency bands, the metal behaves as a dispersion medium with a huge loss with the frequency increases [84]. In order to obtain ideal transmission efficiency in high-frequency bands, all-dielectric designs are a valid route. Dielectric resonant metamaterial resonances are Mie resonances, and the confinement of the fields is not deep-subwavelength-like metallic systems, dielectric particles contain abundant multipole high-Q resonances, which can be widely used as DMs [85], [86], [87]. Zhang et al. [88] proposed an all-dielectric EIT-like metamaterial that operates under magnetic field excitation. It is composed of two ceramic materials. Barium strontium titanate (BST) is used as the bright mode, and calcium titanate ($CaTiO_3$) is used as the DM. Fig. 6(g) illustrates the unit cell of the metamaterial, which is formed by orthogonal stacking of BST and $CaTiO_3$. Since there is no ohmic loss caused by metal, the loss factor of a dielectric resonator is mainly determined by the dielectric loss. When the magnetic field perpendicular to the BST is incident, it can be observed that a significant absorption drop is produced at 8.9 GHz. Apparently, the narrow transmission window is caused by the splitting of the original dip of the bright-dark mode resonator due to the local field coupling effect.

C. Analogous EIT in THz Bands

Metamaterials have attracted a lot of attention in the THz spectral regime due to their unique properties and potential applications. One of the main advantages of THz metamaterials is that they can manipulate the THz waves in unprecedented ways. For instance, they can be used to create artificial materials with negative refractive indices, which do not exist in nature. Metamaterials can also be used to enhance the sensitivity of THz sensors, making them more suitable for applications such as security screening, medical imaging, and environmental monitoring [89].

In addition to improving efficiency, researchers are also investigating ways to enhance the Q factor of THz metamaterials. In 2012, Al-Naib [90] proposed a mirrored arrangement of asymmetric single ASRs that dramatically enhance the Q factor of the inductive–capacitive resonance. The proposed structure is shown in Fig. 7(a). When the electric field polarized along the y-axis is incident, the simulated results are shown in Fig. 7(b). The Q factor of nonmirrored metamaterial is 7.8 but can reach up to 24.2 in the mirrored metamaterial. The mirrored structure is found to support antiphase currents in the metamaterial at the LC resonance. The out-of-phase current oscillations suppress the radiation due to the cancellation of the net dipole moment and allow the LC mode to become subradiant. The radiation property of this excitation is controlled by the degree of asymmetry of the gap position in the individual resonators. Polarization-independent metamaterials have also been extensively studied in THz metamaterials. In 2013, Zhang et al. [91] proposed a polarization-independent PIT metamaterial, as shown in Fig. 7(c). In the proposed structure, they find four different modes that contribute to the PIT resonance band, namely, a superradiant mode (SM), a super-DM, a subradiant mode (sM), and a subdark mode (dM). It is the coupling among these four modes, which leads to the PIT effect, and the simulation and experiment results are shown in Fig. 7(d). Xu et al. [92] proposed a metamaterial composed of a CW and a pair of circular split rings (CSRs), as shown in Fig. 7(e). The CW and CSRs are chosen as the bright mode and DM. The near-field coupling between CW and CSRs excites the induction–capacitance resonance mode inside the CSRs, which induces the EIT-like effect. Moreover, increasing the radius size of the CSR, the transparent window gradually switches from the symmetric Lorentz window to the asymmetric Fano window. Xu et al. [32] proposed a spoof LSP structure in the THz range, as shown in Fig. 7(f). The bright broadband dipole mode covers multiple dark spoof LSP modes to achieve three induced transparent peaks.

An all-dielectric metamaterial is also a good method to improve the modulation depth and Q factor, so all-dielectric resonators have great potential in the THz range. In 2019, Ma et al. [93] proposed a silicon-based metamaterial with an EIT-like effect at THz frequencies, as shown in Fig. 7(g). The unit cell consists of two asymmetric SRRs (a-SRRs), whose asymmetric properties arise from their differing arc lengths. They theoretically proved and verified experimentally that the metamaterial could exhibit high transmittance and large group delay. The transparent window of the system is caused by the interaction of two bright modes caused by the simultaneous excitation of magnetic moments within the same cell. Similar to the behavior of metallic structures, all-dielectric metamaterials can also be used to design

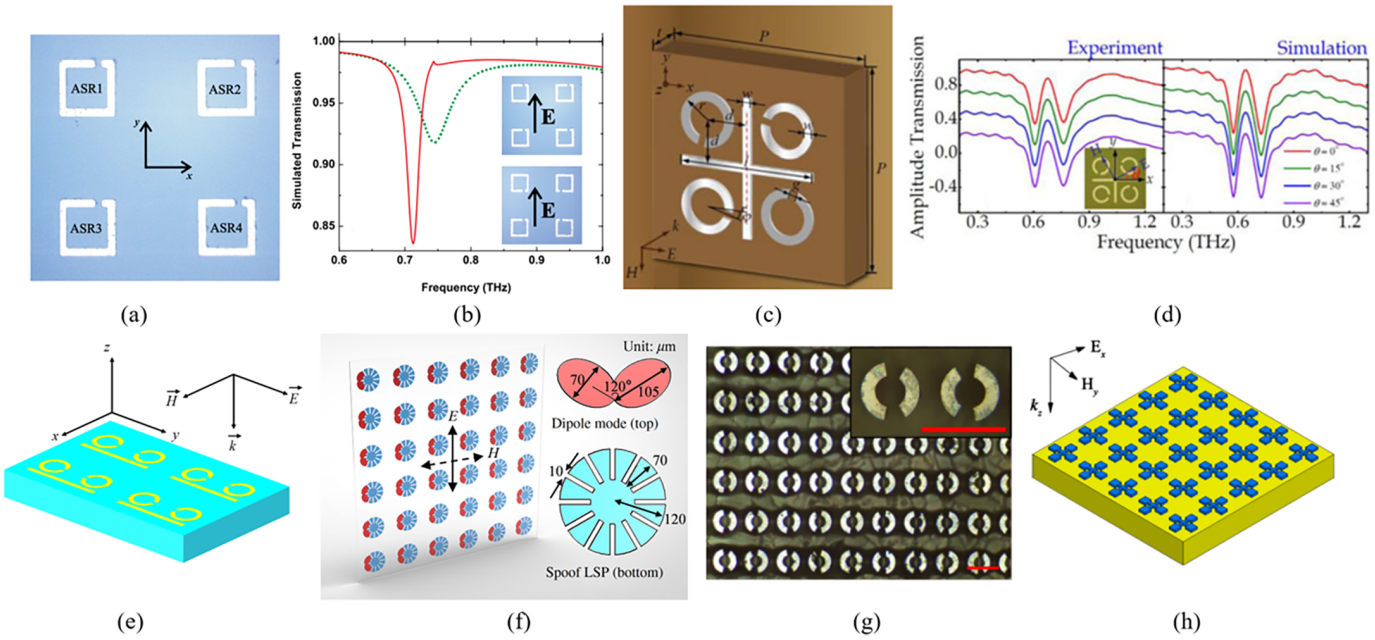

Fig. 7. (a) Optical microscopic images of the fabricated metamaterial structures and (b) simulated transmission spectra [90]. (c) Schematics of a PIT c-SRR unit cell. (d) Experimental and simulated transmission amplitudes [91]. (e) Structure of metallic metasurface to realize double transparent peaks [92]. (f) Multiple spoof LSP metasurface [32]. All-dielectric EIT-like metamaterials: (g) a-SRRs dielectric metamaterial [93]. (h) Windmill-shape metamaterial [63].

polarization-insensitive structures. Zhang et al. [63] designed a polarization-insensitive all-dielectric EIT-like metamaterial. The structure is a windmill-type dielectric structure, as shown in Fig. 7(h). Instead of isolated dark and bright modes, the unit cell is a unified structure composed of two orthogonal dumbbell dielectric resonators. Numerical results show that a typical EIT-like transmission peak accompanied by a large group index appears near 0.5 THz. With the angle change of incident waves, the transmission spectrum has little difference, which proves the polarization insensitivity.

D. Analogous EIT in Optical Bands

In 2008, Zhang et al. [22] proposed the concept of EIT metamaterial for the first time, as shown in Fig. 8(a). They used short wires parallel to the incident electric field as the bright mode and a pair of short metal wires perpendicular to the incident electric field as the DM. d represents the distance between bright mode and DM. As shown in Fig. 8(b), the interference between bright and dark resonant elements makes the spectrum of the imaginary part of the electric field appear as obvious depressions, and the depth and width of the depressions vary with the distance. Meanwhile, the real part of the electric field is highly dispersed at the transparent resonant frequency, which indicates that the light pulse propagates at an extremely low group velocity. When the bright and dark elements are coupled, the electromagnetic field is disturbed, and the bright-mode resonance is suppressed. In 2009, Liu et al. [94] proposed a stacked structure, as shown in Fig. 8(c). The structure consists of two gold bars placed parallel at the bottom, a gold bar placed vertically above the former, and the three form an H shape. Among them, the top gold bar is used as a broadband dipole antenna, and the bottom gold bar is used as a nonradiating quadrupole antenna. Fig. 8(d) shows the transmission and reflection spectrum, where a transparent peak appears around 170 THz.

When the metallic structure resonates, the ohmic loss has a great impact on the Q factor, especially in the far-infrared band. Therefore, a Si-based array was proposed in [95], as shown in Fig. 8(e), which minimizes the damping and results in a sharp resonance peak with the Q value as high as 483 at the wavelength of 1376 nm. Measured results are shown in Fig. 8(f). In terms of sensing applications, as the refractive index ranges from 1.40 to 1.44, the sensitivity is $S = 289$ nm/RIU, and the FOM value is 103, which exceeds the most records for Fano resonant LSP resonance sensor. With proper design, these metasurfaces can also confine the optical field to the nanoscale region, thus opening up the possibility of biological/chemical sensing, enhanced emission rate, optical modulation, and low loss of slow optical devices.

Optical microcavities have also been found to achieve EIT-like effects. In 2020, Wang et al. [96] used the parity-time symmetric state of optical microcavities to realize the switch control of the EIT-like spectrum. The authors manipulate the switch by exploiting the chiral eigenstates at exceptional points (EPs) in a non-Hermitian system consisting of two microcavities coupled by a waveguide, as shown in Fig. 8(g). The optical microcavity makes the light undergo total reflection on the inner wall to form a whispering gallery mode. At EPs, the chirality of 1 (EP_+) corresponds to the clockwise (CW) eigenmode, and the chirality of -1 (EP_-) corresponds to the counterclockwise (CCW) eigenmode. By adjusting the distance between the two microcavities, the phase of light propagating between the two microcavities can be controlled to achieve destructive interference, which constitutes the EIT-like behavior. There are two energy levels in each cavity due to mode splitting, and the splitting of the transparent

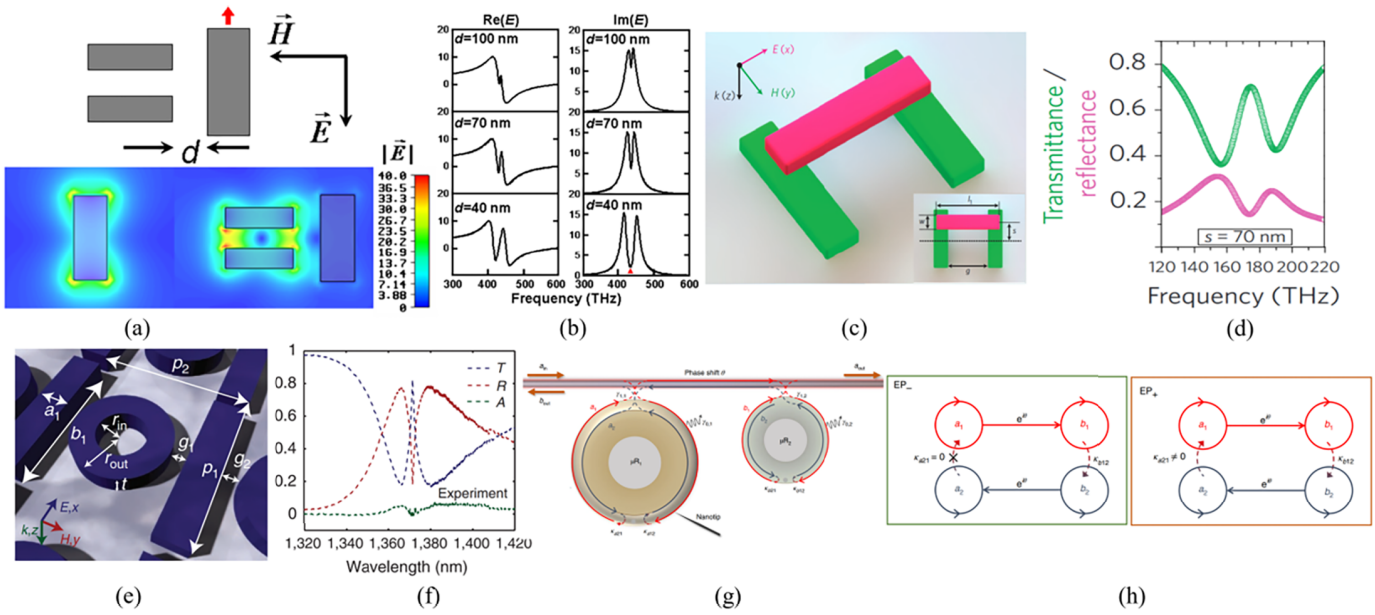

Fig. 8. EIT-like optical metamaterials. (a) Unit cell of the π-shape plasmonic system and the 2-D field of an uncoupled radiative atom (left) and a radiative atom coupled with a dark atom with a separation of 40 nm (right) at a frequency of 428.4 THz. (b) Real part and imaginary part of the electric field with a different distance d [22]. (c) Stacked plasmonic structure and (d) its transmission and reflection spectrum [94]. (e) Si-based metasurface and (f) its measured transmittance, reflectance, and absorption spectra [95]. (g) Microcavities system and (h) its optical path loops with chirality -1 (EP$_-$) and chirality 1 (EP$_+$) [96].

peak occurs. The author modulates the high-Q microtoroid to the EPs by adding a nanotip. When the chirality is -1, the CW mode in the high-Q microtoroid can be coupled to the CCW mode. However, the CCW mode cannot be coupled to the CW mode because the loop is interrupted, and the interference disappears, turning off the EIT-like spectrum. When the chirality is 1 (EP$_+$), the light can be reflected from the CCW mode to the CW mode. Therefore, there is a loop interference in the system, the degeneracy of the EPs makes the transmission spectrum present a single transparent peak, and the EIT-like spectrum is turned on. This work provides a new method for the regulation of EIT-like transmission.

IV. EIT-Like Metamaterial Sensors

EIT-like metamaterials produce sharp resonant peaks and are extremely sensitive to external environment change; therefore, EIT-like structures are widely used in sensors.

A. Basic Concepts of EIT-Like Sensors

The principle of EIT-like metamaterial sensors is based on spectrum shift and change of the Q factor. When detecting different materials under test (MUTs), the different refractive index of MUTs causes the frequency offset of the EIT-like peaks. Moreover, losses of MUTs affect the Q factor and amplitude of the resonant peaks and dips. It should be mentioned that the EIT-like peak is also accompanied by a large group delay; therefore, the amplitude and Q factor of the group delay are also affected by MUTs, which can be used as alternative parameters of the sensor. The sensitivity (S) and figure of merit (FOM) can be used to characterize sensor performance, which can be defined as [97]

$$S = \frac{\Delta\lambda}{\Delta n} \tag{10}$$

$$\text{FOM} = \frac{S}{\text{FWHM}} \tag{11}$$

where $\Delta\lambda$ represents the offset of the wavelength, Δn represents the shift of the refractive index, and FWHM (full-width at half-maximum) represents the 3-dB bandwidth.

In 2012, Meng et al. [98] proposed an EIT-like metasurface, as shown in Fig. 9(a). Meng et al. [98] discussed the potential of refractive index sensing. They plot the spectrum shift in Fig. 9(b) by placing a 4-mm-thick dielectric slab with a relative permittivity ε_r on the surface. The sensitivity of the structure is 77.25 mm/RIU and the FOM of 8.14. This early sensor concept is a simulation analysis without further experiments. In order to reduce the size of the EIT-like sensor, Zhu et al. [99] conducted a theoretical and experimental study on the detuned dipole effect. They loaded a pair of detuned SRR structures on the sides of a microstrip line to achieve an EIT-like spectrum, as shown in Fig. 9(c). The EIT-like structure based on microstrip line coupling can be used as a sensor based on the refractive index change. When the refractive index changes from 1 to 1.48, the simulated and measured spectrum changes are shown in Fig. 9(d). The sensitivity is 14.2 mm/RIU, and the FOM is 6.17.

B. EIT-Like Sensors in Chemistry

EIT-like sensors in the chemical field are mainly designed for detecting various solution concentrations. As shown in Fig. 9(e), Xu et al. [42] reported an EIT-like circuit consisting of an open stub and an SRR resonator, in which the open stub acts as the bright mode, which is excited by

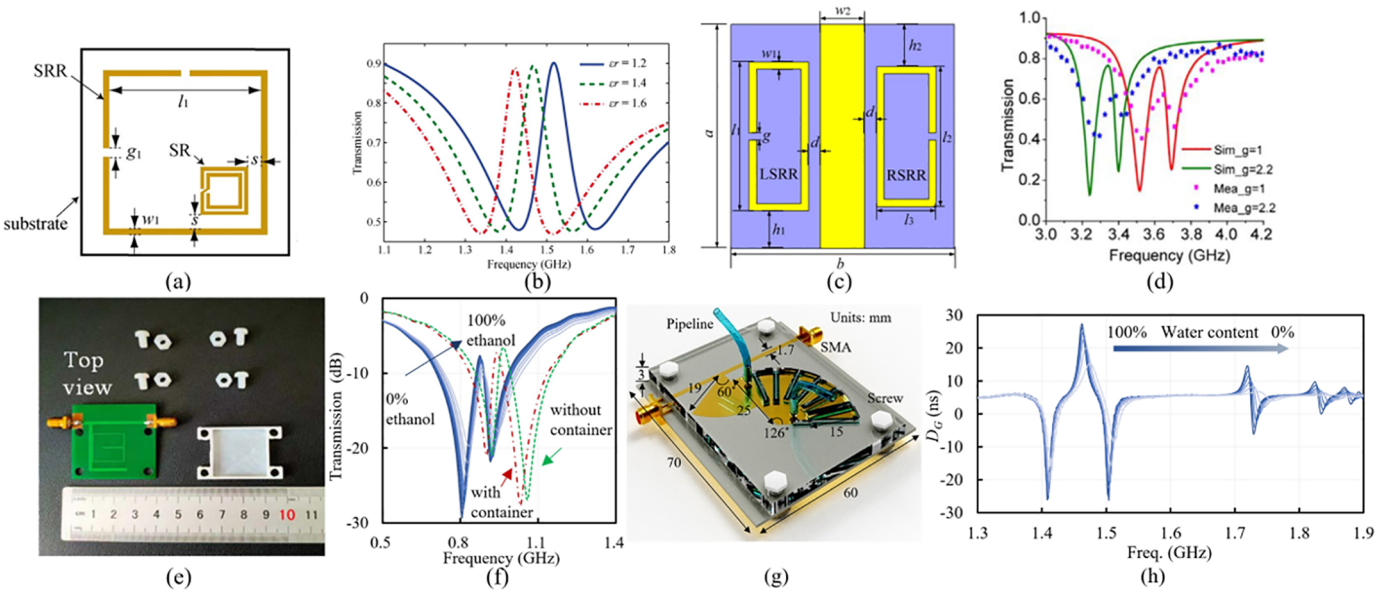

Fig. 9. EIT-Like refractive index sensors. (a) EIT-like metasurface and (b) its varying transmission with the change of permittivity [98]. (c) Detuned magnetic dipoles EIT-like circuit and (d) its varying transmission spectrum with the change of permittivity [99]. EIT-like metamaterial sensors to detect chemical liquids. (e) EIT-like microstrip circuit and (f) its varying spectrum when detecting water–ethanol solutions [42]. (g) Multiple EIT-like sensor based on spoof LSP and (h) its varying group delay spectrum when detecting water–ethanol solutions [32].

the microstrip line directly, and the SRR resonator acts as the DM, which is excited by strong coupling with the open stub. Due to the destructive interference between transmission paths around 960 MHz, a narrowband EIT-like transmission peak is generated. The sensor is applied to measure the complex permittivity of the water–ethanol mixed solutions, and the measured transmission curves are shown in Fig. 9(f). After data processing, the sensitivity of the sensor can reach as high as 5%. The high sensitivity exceeds other sensors based on the single SRR (SSRR) and complementary SRR (CSRR).

In order to detect MUTs at more detecting windows, multiple EIT-like modes are realized in a single sensor [30], [31], [32]. In 2022, Xu et al. [32] developed a plasmonically induced transparency (PIT) sensor structure with three EIT-like modes. Unlike the previous works based on multiple resonators, Xu et al. [32] only use a wideband sector stub and a spoof LSP structure to realize three EIT-like modes, as shown in Fig. 9(g). Through numerical fitting and actual measurement of the structure, the authors used it to measure the complex permittivity of liquids, and the transmission spectrum change is shown in Fig. 9(h). The high sensitivity achieves 4.4%, and the sensor works well at all three EIT-like modes.

C. EIT-Like Sensors in Biomedicine

In biomedicine, EIT-like sensors are usually set in the THz bands. In 2019, Yan et al. [100] proposed a terahertz EIT-like biosensor consisting of a pair of broken-symmetry double SRRs (DSRRs), as shown in Fig. 10(a). Under the radiation of the probe light, a transparent window appears at 1.67 THz, as shown in Fig. 10(b). They implanted oral cancer cell HSC3 into the sensor. When the cell concentration increased from 1×10^5 to 7×10^5 cell/ml, the frequency shift Δf changed from 50 to 90 GHz, which can be shown in Fig. 10(c). The extracted Δf as a function of cell concentration is shown in Fig. 10(d). The maximum sensitivity reaches 900 kHz/cell ml^{-1} at 7×10^5 cells/ml, which means that one cell per milliliter results in a frequency shift of 900 kHz. In addition, apoptosis can also be monitored by changes in Δf. As the anticancer drug concentration increased from 1 to 15 μm, the drug action time was extended from 24 to 72 h, and Δf varied in the range of 140–70 and 140–40 GHz, respectively. This EIT-like biosensor has essential application prospects in the field of biomedicine. In 2021, Zhang et al. [44] proposed a biosensor with an EIT-like structure to classify and detect glioma cell molecules.

In order to achieve polarization-independent characteristics, CWs and SRRs were used for structural design, as shown in Fig. 10(e). The EIT-like window appeared at 2.24 THz under the incidence of both x- and y-polarized waves, as shown in Fig. 10(f). To further characterize the sensing performance, two types of glioma cells (mutant and wild-type) were cultured and adhered to the metal surface of the proposed metamaterial biosensor. The frequency response and amplitude response of cells with different concentrations were obtained by measuring the transmission spectrum. When the wild-type glioma cells were at 8×10^5 cell/ml, the experimental sensitivity can reach up to 248.75 kHz/cell ml^{-1}, and the sensitivity of the sensor can reach 496.04 GHz/RIU, which is far more than any other structure of THz sensor [101]. The sensor was successfully used to distinguish different types of cells. By analyzing the terahertz spectra of the biosensor covered by mutant and wild-type glioma cells at the same concentration (4×10^5 cells/ml), it was found that the resonance frequencies of the two glioma cells were significantly different, as shown in Fig. 10(g), indicating that the biosensor realized the recognition of cancer cells at a specific cell concentration. In order to have a better

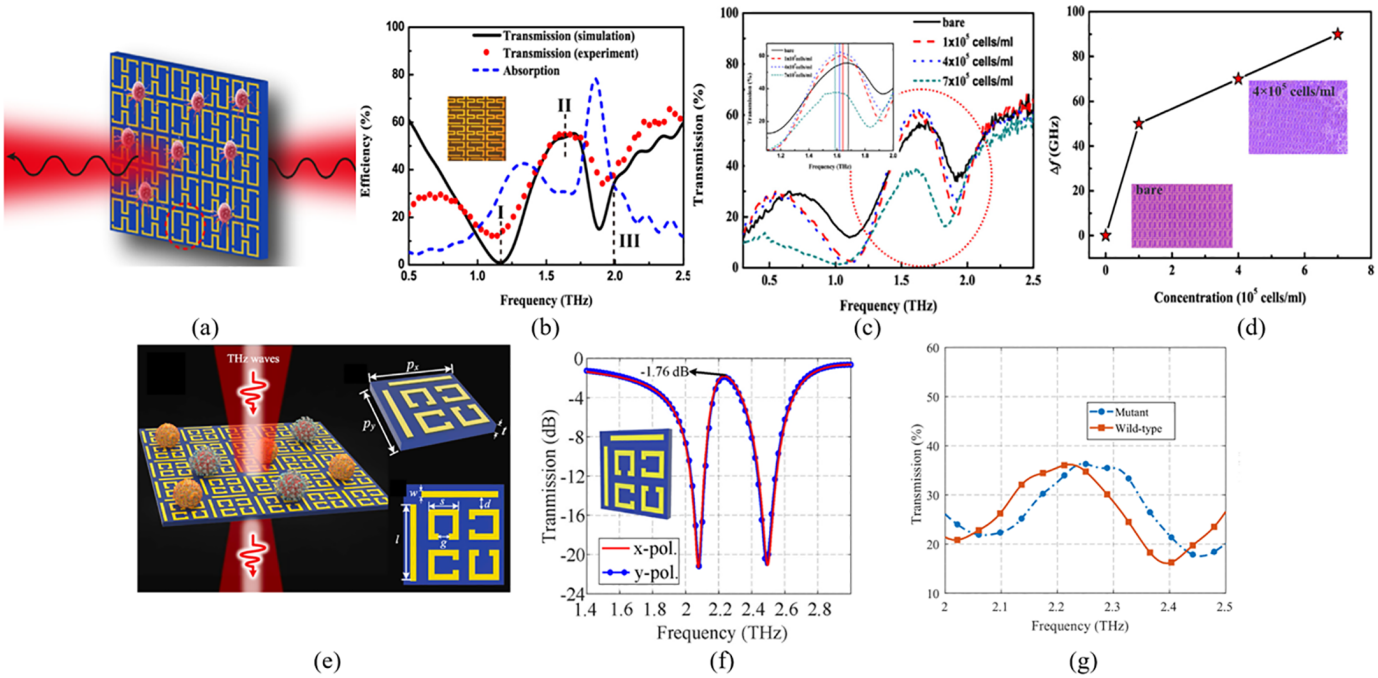

Fig. 10. EIT-like metasurface biosensors. (a) Double-SRRs metasurface sensor with broken symmetry and (b) its transmission without samples and (c) under different cancer cell concentrations from 1×10^5 to 7×10^5 cells/ml. (d) Frequency shift Δf with different concentrations [100]. (e) Biosensor with four different opening directions SRRs, and (f) its transmission under *x*- and *y*-polarized incident waves. (g) Measured transmission of two types of cells with the same cells concentration of 4×10^5 cells/ml [44].

TABLE I
VARIOUS EIT-LIKE METAMATERIAL SENSORS

Ref.	Structure	Frequency	Sensitivity	FOM
26	Si-patch	310 THz	294 nm/RIU	42
32	Sector-LSP	1.49 GHz,1.76 GHz,1.92 GHz	15.58 mm/RIU	42.05
35	Au-grating	171 THz	588 nm/RIU	3.8
37	Plasmonic metasurface	183.8 THz	497.8 nm/RIU	480
39	Active SRR	1.48 GHz	0.012 pF/ns	-
42	Stub-SRR	0.98 GHz	56.04 mm/RIU	4.38
95	Si-patch	218 THz	289 nm/RIU	103
98	SRs-SRRs	1.56 GHz	77.25 mm/RIU	8.14
99	CW-SRRs	3.64 GHz	14.2 mm/RIU	6.17
125	InSb slot waveguide	1 THz	427.5 nm/℃	-
128	Graphene-grating	6.4 THz	160 nm/K	-

comparison between various EIT-like sensors, we list some specific structures and parameters in Table I.

V. MODULATION OF EIT-LIKE METAMATERIALS

How to realize the dynamic modulation of the EIT-like metamaterials has become a hot issue in recent years. Various dynamic modulation technologies have been developed, including graphene modulation, temperature modulation, photosensitive modulation, electrical modulation, and microelectromechanical system (MEMS) modulation.

A. Graphene Modulation

Metamaterials of graphene are attracting intense attention [102], [103], [104], [105], [106], [107]. Graphene has the advantages of single-atom thickness, high electron mobility, and adjustable carrier density. Its conductivity can be dynamically tuned through the applied electric field, affecting its Fermi level [108], [109], [110]. The relative permittivity of graphene can be expressed as

$$\varepsilon_r(\omega) = 1 + \frac{j\sigma(\omega)}{\omega\varepsilon_0 t} \tag{12}$$

where t and $\sigma(\omega)$ are the thickness and conductivity of graphene, ω is the angular frequency, and ε_0 is the vacuum permittivity. The conductivity of graphene in vacuum $\sigma(\omega)$ can be expressed as [110], [111]

$$\sigma(\omega) = j\frac{e^2 k_B T\left(\frac{E_F}{k_B T} + 2\ln\left(e^{-\frac{E_F}{k_B T}} + 1\right)\right)}{\pi\hbar^2(\omega + j\tau^{-1})} \tag{13}$$

where k_B, $\hbar$, and e are Boltzmann's constant, reduced Planck's constant, and electron charge, respectively. E_F is the Fermi

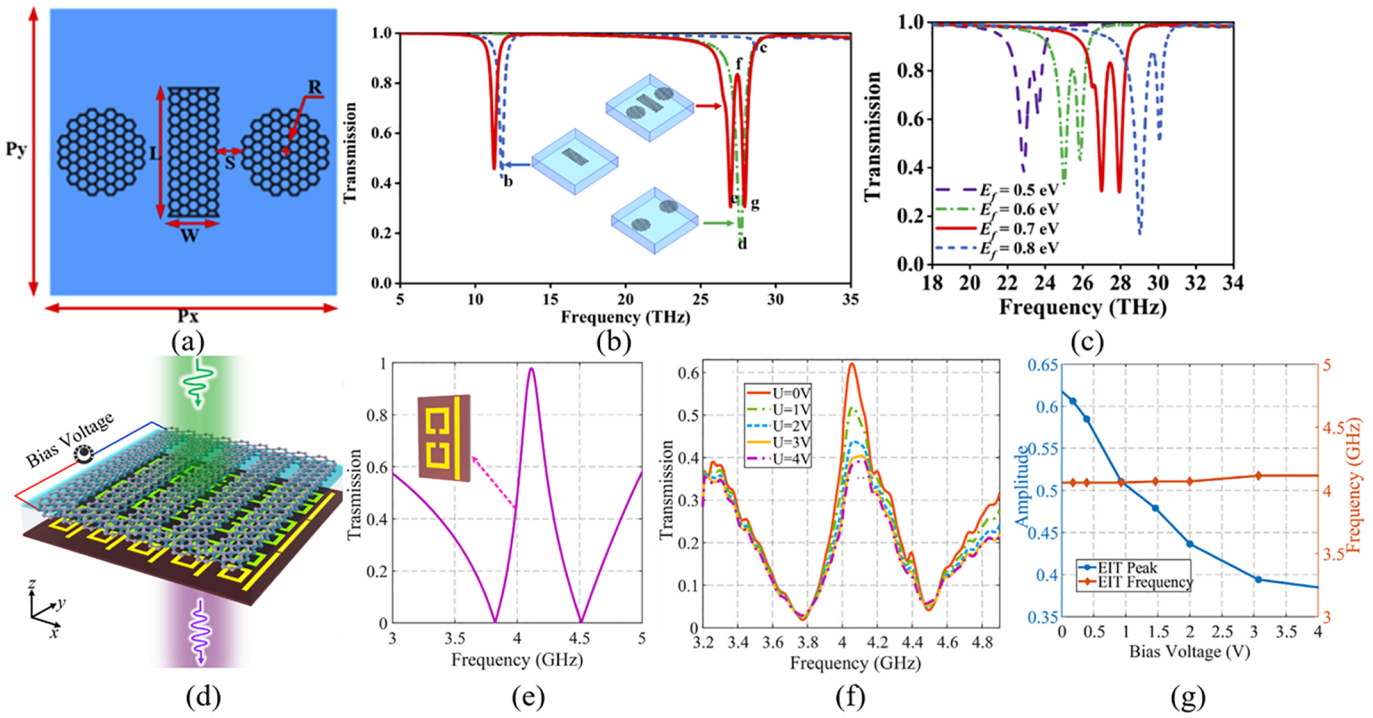

Fig. 11. Graphene-based modulated EIT-like metamaterials. (a) Structure with nanodisks and nanostrip and (b) its transmission spectra of the disk, strip, and the EIT-like metamaterials. (c) Transmission at various Fermi levels of the graphene [112]. (d) CWR-SRRs' graphene-based metamaterial and its transmission (e) without graphene and (f) with graphene under different bias voltages. (g) EIT-like peak and resonate frequency as functions of bias voltages [107].

level, T is the temperature, and τ is the relaxation time. The relaxation time can be further described as $\tau = \mu E_F/(ev_f^2)$, where v_f is the Fermi velocity and μ is the electron mobility. Therefore, the permittivity of graphene can be actively tuned by changing its Fermi energy. Once the bias voltage changes, the Fermi energy level of graphene changes, which in turn leads to a change in the relative permittivity.

Xiao et al. [112] proposed a graphene-based metasurface at mid-infrared frequencies, as shown in Fig. 11(a). The structure comprises two subwavelength monolayer graphene nanodisks coupled with a monolayer graphene nanostrip. The coupling of the dipole resonance with the quadrupole resonance of the nanoribbon can generate two split resonances with EIT-like windows at the desired frequency. The spectrum is shown in Fig. 11(b). They further adjusted the Fermi level of graphene through bias voltage to tune the EIT-like response dynamically, as shown in Fig. 11(c). In addition, the potential of this structure as a sensor for the refractive index of a medium is analyzed, the sensitivity can reach 3016.7 nm/RIU, and the FOM exceeds 12.

Graphene has many attractive properties at terahertz frequencies, but the nearly resistive impedance of graphene limits the development of EIT-like microwave metamaterials. In 2021, Zhang et al. [107] experimentally integrated graphene into a microwave metamaterial. The structure is a striped graphene-based sandwich structure (GSS), as shown in Fig. 11(d). In the absence of GSS, the EIT-like peak can be observed at 4.1 GHz, as shown in Fig. 11(e). The cut wire resonator (CWR) and SRRs act as the bright mode and DM, respectively. By applying a bias voltage to the graphene layer, the surface impedance changes significantly, affecting the resonance strength of the DM. The experimental results show that the graphene can achieve dynamic control of the EIT peak at relatively low bias voltages. Fig. 11(f) and (g) shows the measured EIT-like spectra of graphene metamaterials at different bias voltages. The resonant frequency of the metamaterial does not change with the bias voltage change, which indicates that the structure can achieve continuous tuning of the EIT-like strength under the condition that only the DM damping is affected.

B. Optical Modulation

Optical modulation changes the material's electrical conductivity by adjusting the laser intensity [113], [114], [115], [116]. As the light intensity increases, the photocarrier concentration inside the photosensitive material changes, changing its electrical conductivity. In this study, both Si and GaAs have been found to be good photosensitive materials for all-optical modulation [117], [118], [119], [120], [121].

The photosensitive properties of Si can be used to build optical switches. Manjappa et al. [122] proposed a silicon-implanted terahertz asymmetric metallic split-ring (Si-TASR) metamaterial where the conductivity of Si is used for dynamic modulation. As shown in Fig. 12(a), the metamaterial consists of a sapphire substrate, Si film, and an aluminum resonant ring. The Si film with a thickness of 200 nm is used as an active optical switch. Without the pumping laser, the evident Fano resonance phenomenon can be observed; however, with the increase in the pumping laser intensity, the intensity of the Fano resonance weakens. When the power increases to 40 W (140 μJ/cm^{-2}), the resonance completely disappears, as shown in Fig. 12(b). As the pumping laser power increases,

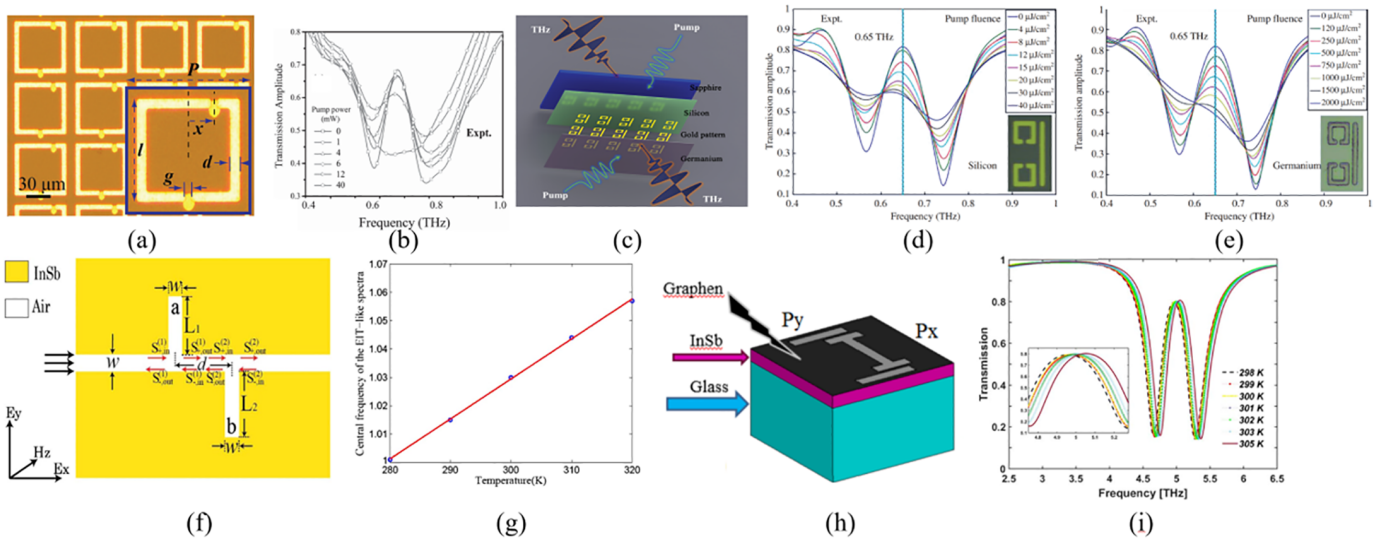

Fig. 12. Optically modulated EIT-like metamaterials. (a) Si-TASR sample and (b) its tunable transmission spectrum [122]. (c) Si-Ge metamaterial and change of EIT-like peak at 0.65 THz by changing the photoconductivity of (d) Si and (e) Ge films [124]. EIT-like temperature sensors. (f) InSb sensor and (g) its central frequency of the EIT-like transmission as a function of temperature [125]. (h) H-shape InSb structure and (i) its transmission change with the temperature [128].

the number of excited carriers in Si increases, and at a power of 40 W, the semiconductor Si layer behaves like a metalloid, resulting in the Fano resonances completely being switched OFF.

Germanium (Ge) has also received extensive attention as a photosensitive material. Compared with Si, Ge has higher carrier mobility and more significant intrinsic carrier concentration [123]; thus, the conductivity can be dynamically tuned by changing the carrier concentration through photoexcitation. Zhou et al. [124] established a planar metamaterial consisting of Ge and Si thin films as the active medium, as shown in Fig. 12(c). It has optical reconfiguration and THz modulation characteristics. Fig. 12(d) and (e) shows the amplitude change of the transmission spectrum when optical pulses of different power are transmitted to the two films, respectively. Measured results demonstrate that transmission can be modulated on picosecond and nanosecond timescales; the recovery time for the slow and fast ON–OFF–ON switching cycles is 1.7 ns and 11 ps, respectively, which are mapped as the pump delay time of Si and Ge. The ultrafast all-optical modulation dynamic behavior is attributed to the defects introduced in amorphous Ge, which acts as trap-assisted recombination sites and accelerates carrier relaxation. Equally important, the integrated Si thin film defines a slower speed response and a wider time window, making the device more tolerant to delay time uncertainty while maintaining ultrafast switching. Therefore, EIT-like hybrid devices with multiple photoactive materials have promoted the development of next-generation multifunctional THz components to a certain extent.

C. Temperature Modulation

The complex permittivity of InSb is sensitive to temperature, so devices made of this material can be used to make temperature sensors [125]. The complex permittivity of InSb can be expressed by the Drude model [126]

$$\varepsilon(\omega) = \varepsilon_\infty - \frac{\omega_p^2}{\omega^2 + i\gamma\omega} \tag{14}$$

where ε_∞ is the high-frequency permittivity, ω is the angular frequency, and γ is the damping constant. The plasma frequency $\omega_p = (Ne^2/\varepsilon_0 m^*)^{1/2}$ depends on the intrinsic carrier density N, the electronic charge e, the vacuum permittivity ε_0, and the effective mass $m*$ of the free carriers. The plasma frequency ω_p of InSb increases exponentially with the increase in the temperature, and the intrinsic carrier density N (in m^{-3}) of InSb obeys this relationship [127]

$$N = 5.76 \times 10^{14} T^{1.5} \exp(-0.26/2k_B T) \tag{15}$$

where k_B is Boltzmann's constant and T is the temperature.

In 2015, Liu et al. [125] proposed a coupling model of a double-stub resonator composed of InSb, as shown in Fig. 12(f). When the temperature is constant at 280 K, the resonant frequencies of the two resonators are 0.95 and 1.05 THz. When the two are connected together through a 50-Ω microstrip line, an EIT-like transmission peak is generated at 1 THz. As the temperature increases from 280 K to 320 K, the EIT-like frequency increases from 1 to 1.057 THz, as shown in Fig. 12(g). The calculated sensitivity is 427.5 nm/K; therefore, this structure works as a terahertz temperature sensor. In 2020, Ghafari et al. [128] used graphene and InSb to fabricate a temperature sensor in the THz band by cutting out an H-shaped antenna and a pair of parallel strip antennas on the graphene layer and depositing them on the InSb and glass layers; to achieve the EIT-like effect, the structure is shown in Fig. 12(h), and then, the influence of the thickness of the material layer and the chemical potential of graphene on the results is analyzed. They used the structure to make a temperature sensor, and the results showed that, when the chemical potential of graphene is 0.3 eV, the structure

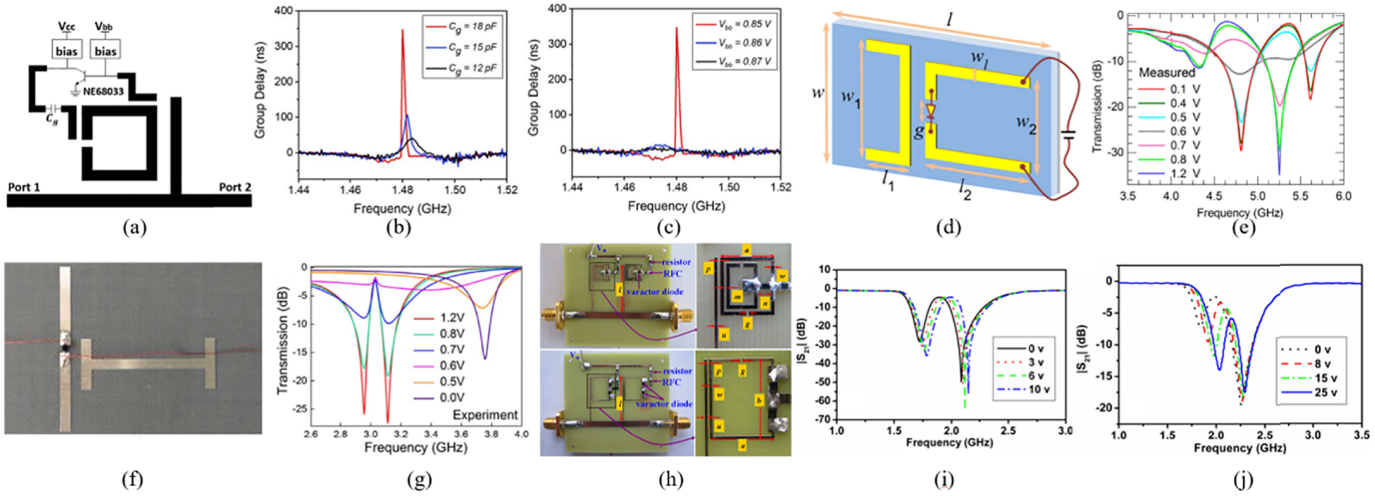

Fig. 13. Electrically modulated EIT-like metamaterials. (a) Active sensor and its group delay changing with (b) value of the sensing capacitor C_g and (c) transistor base voltage V_{bb} [39]. (d) EIT-like tunable metamaterial and (e) its transmission spectrum under different biasing voltages [130]. (f) Symmetry-broken structure and (g) its transmission spectrum [131]. (h) Tunable EIT-like circuits based on DSRR (up) and SSRR (down) and their transmission spectra based on (i) DSRR and (j) SSRR under various bias voltages [132].

can achieve a maximum sensitivity of 160 nm/K, and the spectral shift at the highest sensitivity is shown in Fig. 12(i), respectively.

D. Electrical Modulation

In microwave bands, loading electronic devices are widely used because of the simple fabrication and low cost. In 2018, Lin et al. [39] integrated the active feedback loop into the EIT-like circuit to obtain a large group delay peak. The designed structure is shown in Fig. 13(a). An active feedback loop compensates for losses and improves the Q factor [129]. In this structure, the passive EIT-like structure is composed of an open-circuit stub and SRR resonator, and the active structure is composed of an amplifier and the sensing capacitor. When the sensing capacitor C_g and bias voltage V_{bb} are set to the appropriate value, the group delay can reach 350 ns, as shown in Fig. 13(b) and (c). In 2016, Fan et al. [130] realized an electronically controllable EIT-like metamaterial by loading diodes, as shown in Fig. 13(d). By placing a diode at the gap between a pair of wires, the dynamic control of the EIT-like spectrum can be achieved. When the applied voltage ranges from 0.1 to 1.2 V, the emergence and closure of the EIT-like mode can be observed, as shown in Fig. 13(e). Similar to the principle of [130], Yang et al. [131] proposed tunable symmetry-broken metasurfaces made of orthogonal electric dipolar resonators. The metasurface with vertical and horizontal wires integrates a p-i-n diode, and the p-i-n diode is loaded in the middle of the vertical wires, as shown in Fig. 13(f). Fig. 13(g) shows the change in the transmission when the bias voltage changes from 0 to 1.2 V. Under the high bias voltage, the resistance of the diode is small, and the electric dipole resonance with the vertical wire is strong. It exhibits metallic characteristics, and the EIT-like peak does not change. When the bias voltage gradually decreases, the resistance of the p-i-n diode increases, exhibiting dielectric characteristics, and the resonance frequency shifts. Therefore, the structure can be used as an amplitude modulator under a certain bias voltage range. Feng and Han [132] explored two types of tunable transmission-line (TL) EIT-like metamaterials loaded with varactors. The two structures are based on DSRR and SSRR, as shown in Fig. 13(h), where the tunability comes from the controllable characteristics of varactors. For tunable DSRR TL EIT-like metamaterials, the maximum transmittance is independent of the movement of the transparent window. In contrast, for tunable SSRR TL EIT-like metamaterials, the maximum transmittance increases with the transparent window gradually decreasing as the transparent window moves toward the center of the absorption band, as shown in Fig. 13(i) and (j). The energy loss caused by the resistance of the varactor is the main reason for the decrease in the maximum transmittance of the transparent window of the tunable SSRR TL EIT-like metamaterials.

E. MEMS Modulation

Structurally reconfigurable metamaterials based on MEMSs are considered to be the most direct method to achieve active control of metamaterials. MEMS systems have the advantages of low power consumption and fast response, and only a small driving force is required; therefore, tunable EIT-like devices based on MEMS control have also been a hot topic in recent years [133], [134], [135], [136], [137]. In 2016, Pitchppa et al. [133] proposed an MEMS metamaterial whose structural bending angle can be controlled by the driving voltage. The ON and OFFstates of the structure are shown in Fig. 14(a) and (b). The state when no voltage is applied is defined as the OFF state, and when the applied voltage exceeds the rated voltage, it is defined as the ON state. By actively modulating the switch, it is found that 50% EIT-like modulation depth and 2.5-ps group delay can be achieved at 0.68 THz, as shown in Fig. 14(c) and (d). Considering the miniaturized structure and easy integration, the proposed MEMS metamaterial is an ideal candidate for slow-light THz devices, such as modulators, buffers, and optical delays. In 2020, Huang et al. [134] proposed another MEMS control system, as shown in Fig. 14(e).

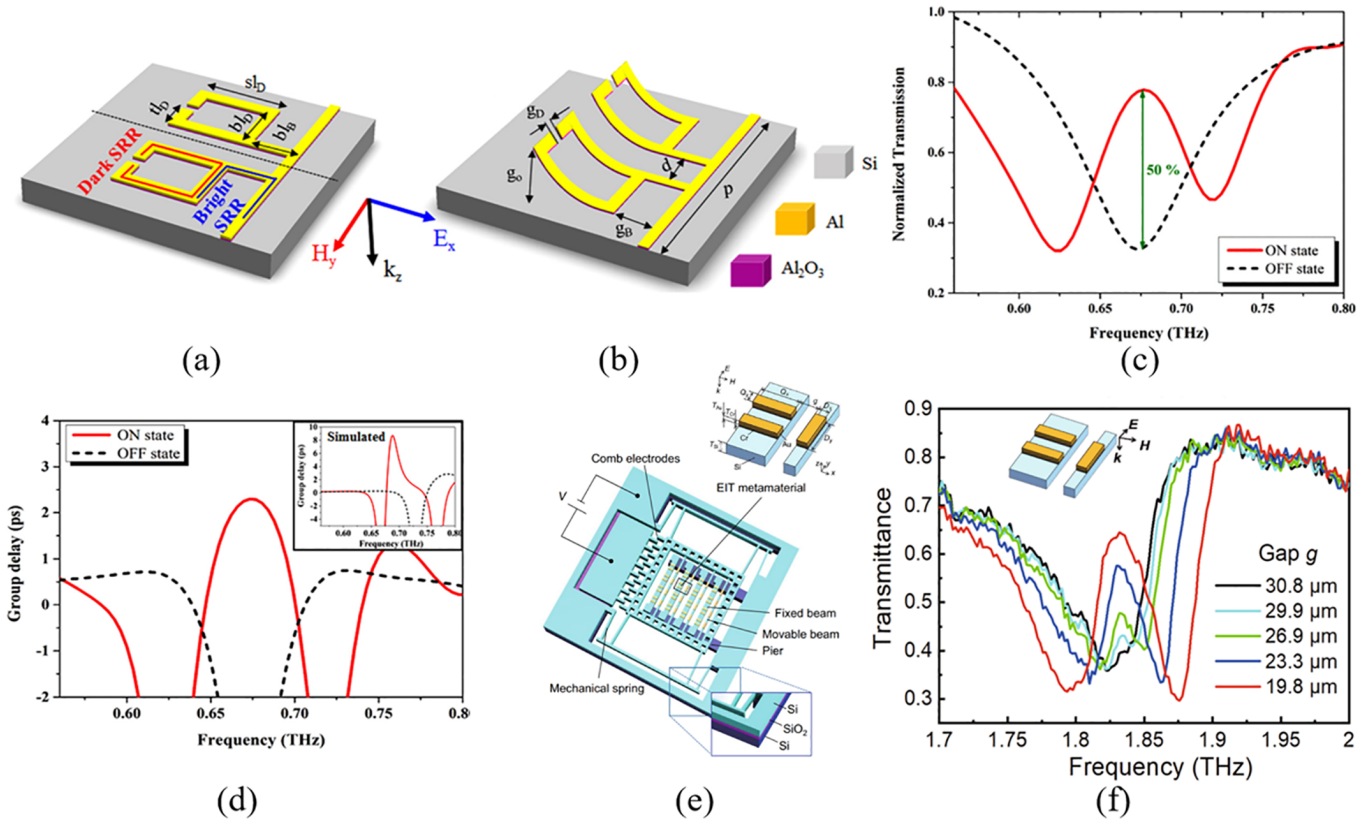

Fig. 14. MEMS modulated EIT-like metamaterials. The coupled MEMS metamaterial in (a) ON state, (b) OFF state, (c) measured transmission, and (d) group delay in the OFF state and ON state [133]. (e) MEMS integrated EIT-like device and (f) measured transmission [134].

By applying a driving voltage to the system, they adjusted the coupling distance between the bright mode and DM, and the modulation of the transmission spectrum is achieved. The modulation spectra under different coupling distances are shown in Fig. 14(f). Experimental results demonstrate that a modulation rate of 38.8% can be achieved by applying a driving voltage. The structure is promising for terahertz optical switches, terahertz communications, and other terahertz wave-related applications.

VI. Outlook

Although EIT-like metamaterials have achieved significant development, some challenging issues deserve attention. First, the metallic loss due to the coupling oscillation between metallic resonators plays a negative role in high-frequency bands, suppressing the Q value and the EIT-like transmission efficiency. As an alternative method to solve this challenge, all-dielectric resonators have the advantages of high dielectric constant and low intrinsic loss; therefore, designing all-dielectric structures offers an alternative method to achieve low-loss and high Q EIT-like metamaterials. However, the shape of all-dielectric structures is limited due to the fabrication process. Combining simple dielectric structures, such as spheres and cubes, to realize a fruitful EIT-like spectrum is an interesting topic. Second, active materials, such as graphene, Si, and InSb, have been widely used to design metamaterials. Developing new semiconductor materials is always a research focus. In recent years, emerging active materials, such as MoS_2 and perovskite [138], have attracted great interest. How to timely explore the application of these new materials in EIT-like metamaterials is a research direction. Finally, the design process of EIT-like metamaterials is time-consuming, accompanied by large-scale parameter optimization. Various intelligent algorithms have been used in metamaterial designs in recent years. Artificial intelligence shows fast design speed and high precision compared to manual tuning, promising for quickly designing and optimizing EIT-like metamaterials [139].

Topological photonic crystal devices have gained significant attention as a transformative technology in recent years [80], [140], [141], In addition to their technological advancements, topological photonic cavities have important applications in the sensor field [89]. A promising topic of research in this area is the realization of the EIT phenomenon in photonic crystals. Such research can lead to the development of higher Q and more robust resonant sensors, thus increasing the accuracy and sensitivity of the devices. On the other hand, optical fiber sensors have also seen significant advancements due to the introduction of photonic crystal fiber's air holes, which permits the insertion of liquid or gas samples into the fibers. This enables a controlled interaction between confined light and sensing samples, leading to the development of novel sensing applications that were previously inconceivable with conventional optical fibers [142], [143], [144], [145]. An interesting direction for future exploration is the EIT sensing technology of optical fiber transmission systems. This

can further improve the sensitivity of fiber optic sensors and bring about new opportunities for advancements in sensing technology.

VII. Conclusion

This article provides a comprehensive review of the research progress of EIT-like metamaterials. First, we introduce the mechanism of EIT coupling using the atomic energy level model and the mechanical oscillator model. Next, we cover various structure designs that span different frequency bands. In addition, we review EIT-like sensors and tunable technologies, such as chemical sensors, biomedicine sensors, graphene modulation, light modulation, temperature modulation, electrical modulation, and MEMS modulation. The development of these dynamic modulations has made significant progress in the creation of controllable optical switches and slow-light devices. Overall, this article aims to provide a detailed overview of the current state of research on EIT-like metamaterials, their designs, and their applications in the field of sensing and tunable technologies.

References

[1] M. Fleischhauer, A. Imamoglu, and J. P. Marangos, "Electromagnetically induced transparency: Optics in coherent media," *Rev. Mod. Phys.*, vol. 77, no. 2, pp. 633–673, Jul. 2005, doi: 10.1103/RevModPhys.77.633.

[2] S. E. Harris, "Electromagnetically induced transparency," *Phys. Today*, vol. 50, no. 7, pp. 36–42, Jul. 1997, doi: 10.1063/1.881806.

[3] S. E. Harris, J. E. Field, and A. Imamoğlu, "Nonlinear optical processes using electromagnetically induced transparency," *Phys. Rev. Lett.*, vol. 64, no. 10, pp. 1107–1110, Mar. 1990, doi: 10.1103/PhysRevLett.64.1107.

[4] K.-J. Boller, A. Imamoğlu, and S. E. Harris, "Observation of electromagnetically induced transparency," *Phys. Rev. Lett.*, vol. 66, no. 20, pp. 2593–2596, May 1991, doi: 10.1103/PhysRevLett.66.2593.

[5] S. Han, R. Singh, L. Cong, and H. Yang, "Engineering the Fano resonance and electromagnetically induced transparency in near-field coupled bright and dark metamaterial," *J. Phys. D, Appl. Phys.*, vol. 48, no. 3, Jan. 2015, Art. no. 035104, doi: 10.1088/0022-3727/48/3/035104.

[6] J. Gu et al., "Active control of electromagnetically induced transparency analogue in terahertz metamaterials," *Nature Commun.*, vol. 3, no. 1, p. 1151, Jan. 2012, doi: 10.1038/ncomms2153.

[7] C. Kurter et al., "Classical analogue of electromagnetically induced transparency with a metal-superconductor hybrid metamaterial," *Phys. Rev. Lett.*, vol. 107, no. 4, Jul. 2011, Art. no. 043901, doi: 10.1103/PhysRevLett.107.043901.

[8] S.-Y. Chiam, R. Singh, C. Rockstuhl, F. Lederer, W. Zhang, and A. A. Bettiol, "Analogue of electromagnetically induced transparency in a terahertz metamaterial," *Phys. Rev. B, Condens. Matter*, vol. 80, no. 15, Oct. 2009, Art. no. 153103, doi: 10.1103/PhysRevB.80.153103.

[9] K. Totsuka, N. Kobayashi, and M. Tomita, "Slow light in coupled-resonator-induced transparency," *Phys. Rev. Lett.*, vol. 98, no. 21, May 2007, Art. no. 213904, doi: 10.1103/PhysRevLett.98.213904.

[10] H. Lu, X. Liu, and D. Mao, "Plasmonic analog of electromagnetically induced transparency in multi-nanoresonator-coupled waveguide systems," *Phys. Rev. A, Gen. Phys.*, vol. 85, May 2012, Art. no. 053803, doi: 10.1103/PhysRevA.85.053803.

[11] M. Amin, R. Ramzan, and O. Siddiqui, "Slow wave applications of electromagnetically induced transparency in microstrip resonator," *Sci. Rep.*, vol. 8, no. 1, p. 2357, Feb. 2018, doi: 10.1038/s41598-018-20771-w.

[12] C. Du et al., "Active control scattering manipulation for realization of switchable EIT-like response metamaterial," *Opt. Commun.*, vol. 483, Mar. 2021, Art. no. 126664, doi: 10.1016/j.optcom.2020.126664.

[13] X.-G. Yin, M.-Q. Wu, Y.-W. Liu, and C.-P. Huang, "A planar metamaterial based on metallic rectangular-ring pair for narrow electromagnetically induced transparency-like effect," *J. Appl. Phys.*, vol. 128, no. 6, Aug. 2020, Art. no. 065105, doi: 10.1063/5.0012575.

[14] M. Fleischhauer and M. D. Lukin, "Dark-state polaritons in electromagnetically induced transparency," *Phys. Rev. Lett.*, vol. 84, no. 22, pp. 5094–5097, May 2000, doi: 10.1103/PhysRevLett.84.5094.

[15] L. V. Hau, S. E. Harris, Z. Dutton, and C. H. Behroozi, "Light speed reduction to 17 metres per second in an ultracold atomic gas," *Nature*, vol. 397, no. 6720, pp. 594–598, 1999, doi: 10.1038/17561.

[16] M. Bajcsy, A. S. Zibrov, and M. D. Lukin, "Stationary pulses of light in an atomic medium," *Nature*, vol. 426, no. 6967, pp. 638–641, Dec. 2003.

[17] C. Liu, Z. Dutton, C. H. Behroozi, and L. V. Hau, "Observation of coherent optical information storage in an atomic medium using halted light pulses," *Nature*, vol. 409, pp. 490–493, Jan. 2001, doi: 10.1038/35054017.

[18] R. Santra, E. Arimondo, T. Ido, C. H. Greene, and J. Ye, "High-accuracy optical clock via three-level coherence in neutral bosonic ^{88}Sr," *Phys. Rev. Lett.*, vol. 94, no. 17, May 2005, Art. no. 173002, doi: 10.1103/PhysRevLett.94.173002.

[19] A. K. Mohapatra, T. R. Jackson, and C. S. Adams, "Coherent optical detection of highly excited Rydberg states using electromagnetically induced transparency," *Phys. Rev. Lett.*, vol. 98, no. 11, Mar. 2007, Art. no. 113003, doi: 10.1103/PhysRevLett.98.113003.

[20] C. Buth, R. Santra, and L. Young, "Electromagnetically induced transparency for X rays," *Phys. Rev. Lett.*, vol. 98, no. 25, Jun. 2007, Art. no. 253001, doi: 10.1103/PhysRevLett.98.253001.

[21] Z.-K. Liu et al., "Deep learning enhanced Rydberg multifrequency microwave recognition," *Nature Commun.*, vol. 13, no. 1, p. 1997, Apr. 2022, doi: 10.1038/s41467-022-29686-7.

[22] S. Zhang, D. A. Genov, Y. Wang, M. Liu, and X. Zhang, "Plasmon-induced transparency in metamaterials," *Phys. Rev. Lett.*, vol. 101, no. 4, Jul. 2008, Art. no. 047401, doi: 10.1103/PhysRevLett.101.047401.

[23] H.-M. Li and F. Xue, "Tailoring polarization of electromagnetically induced transparency based on non-centrosymmetric metasurfaces," *Phys. Lett. A*, vol. 381, no. 35, pp. 3000–3004, Sep. 2017, doi: 10.1016/j.physleta.2017.07.025.

[24] F. Zhang et al., "Large group index induced by asymmetric split ring resonator dimer," *Appl. Phys. Lett.*, vol. 103, no. 22, Nov. 2013, Art. no. 221904, doi: 10.1063/1.4833817.

[25] L. Zhu et al., "A low-loss electromagnetically induced transparency (EIT) metamaterial based on coupling between electric and toroidal dipoles," *RSC Adv.*, vol. 7, no. 88, pp. 55897–55904, 2017, doi: 10.1039/C7RA11175D.

[26] Z. Wei et al., "Analogue electromagnetically induced transparency based on low-loss metamaterial and its application in nanosensor and slow-light device," *Plasmonics*, vol. 12, no. 3, pp. 641–647, Jun. 2017, doi: 10.1007/s11468-016-0309-z.

[27] F. Bagci and B. Akaoglu, "A polarization independent electromagnetically induced transparency-like metamaterial with large group delay and delay-bandwidth product," *J. Appl. Phys.*, vol. 123, no. 17, May 2018, Art. no. 173101, doi: 10.1063/1.5023684.

[28] L. Zhu, F.-Y. Meng, J.-H. Fu, and Q. Wu, "An electromagnetically induced transparency metamaterial with polarization insensitivity based on multi-quasi-dark modes," *J. Phys. D, Appl. Phys.*, vol. 45, no. 44, Nov. 2012, Art. no. 445105, doi: 10.1088/0022-3727/45/44/445105.

[29] A. Joshi and M. Xiao, "Electromagnetically induced transparency and its dispersion properties in a four-level inverted-Y atomic system," *Phys. Lett. A*, vol. 317, nos. 5–6, pp. 370–377, Oct. 2003, doi: 10.1016/j.physleta.2003.09.010.

[30] O. Tsilipakos, L. Zhang, M. Kafesaki, C. M. Soukoulis, and T. Koschny, "Experimental implementation of achromatic multiresonant metasurface for broadband pulse delay," *ACS Photon.*, vol. 8, no. 6, pp. 1649–1655, Jun. 2021, doi: 10.1021/acsphotonics.1c00025.

[31] S. Liu, Z. Xu, X. Yin, and H. Zhao, "Analog of multiple electromagnetically induced transparency using double-layered metasurfaces," *Sci. Rep.*, vol. 10, no. 1, p. 8469, May 2020, doi: 10.1038/s41598-020-65418-x.

[32] Z. Xu, Y. Wang, J. Chang, and T. J. Cui, "Multiple spoof plasmonically induced transparency for sensing applications," *Phys. Rev. A, Gen. Phys.*, vol. 18, no. 2, Aug. 2022, Art. no. 024035, doi: 10.1103/PhysRevApplied.18.024035.

[33] S. Liu, Z. Xu, X. Yin, and H. Zhao, "High-Q-value classical electromagnetically induced transparency based on dipoles overlapping at spoof localized surface plasmons," *J. Opt. Soc. Amer. B, Opt. Phys.*, vol. 38, no. 4, p. 1156, Apr. 2021, doi: 10.1364/JOSAB.417496.

[34] H.-W. Wu et al., "Multifrequency superscattering with high Q factors from a deep-subwavelength spoof plasmonic structure," *Phys. Rev. B, Condens. Matter*, vol. 100, no. 23, Dec. 2019, Art. no. 235443, doi: 10.1103/PhysRevB.100.235443.

[35] N. Liu et al., "Planar metamaterial analogue of electromagnetically induced transparency for plasmonic sensing," *Nano Lett.*, vol. 10, no. 4, pp. 1103–1107, Apr. 2010, doi: 10.1021/nl902621d.

[36] C.-Y. Chen, I.-W. Un, N.-H. Tai, and T.-J. Yen, "Asymmetric coupling between subradiant and superradiant plasmonic resonances and its enhanced sensing performance," *Opt. Exp.*, vol. 17, no. 17, p. 15372, Aug. 2009, doi: 10.1364/OE.17.015372.

[37] A. Alipour, A. Farmani, and A. Mir, "High sensitivity and tunable nanoscale sensor based on plasmon-induced transparency in plasmonic metasurface," *IEEE Sensors J.*, vol. 18, no. 17, pp. 7047–7054, Sep. 2018, doi: 10.1109/JSEN.2018.2854882.

[38] X. Q. Lin, Z. Chen, J. W. Yu, P. Q. Liu, P. F. Li, and Z. D. Chen, "An EIT-based compact microwave sensor with double sensing functions," *IEEE Sensors J.*, vol. 16, no. 2, pp. 293–298, Jan. 2016, doi: 10.1109/JSEN.2015.2480800.

[39] X. Q. Lin, J. Peng, Z. Chen, J. W. Yu, and X. F. Yang, "A group-delay-based sensor using active EIT-like effect with double sensing applications," *IEEE Sensors J.*, vol. 18, no. 22, pp. 9251–9256, Nov. 2018, doi: 10.1109/JSEN.2018.2868873.

[40] M. Yang et al., "Electromagnetically induced transparency-like metamaterials for detection of lung cancer cells," *Opt. Exp.*, vol. 27, no. 14, p. 19520, Jul. 2019, doi: 10.1364/OE.27.019520.

[41] Z. Chen, X. Q. Lin, Y. H. Yan, F. Xiao, M. T. Khan, and S. Zhang, "Noncontact group-delay-based sensor for metal deformation and crack detection," *IEEE Trans. Ind. Electron.*, vol. 68, no. 8, pp. 7613–7619, Aug. 2021, doi: 10.1109/TIE.2020.3008386.

[42] Z. Xu, Y. Wang, and S. Fang, "Dielectric characterization of liquid mixtures using EIT-like transmission window," *IEEE Sensors J.*, vol. 21, no. 16, pp. 17859–17867, Aug. 2021, doi: 10.1109/JSEN.2021.3085954.

[43] K. V. Sreekanth et al., "Extreme sensitivity biosensing platform based on hyperbolic metamaterials," *Nature Mater.*, vol. 15, no. 6, pp. 621–627, Jun. 2016, doi: 10.1038/nmat4609.

[44] J. Zhang et al., "Highly sensitive detection of malignant glioma cells using metamaterial-inspired THz biosensor based on electromagnetically induced transparency," *Biosensors Bioelectron.*, vol. 185, Aug. 2021, Art. no. 113241, doi: 10.1016/j.bios.2021.113241.

[45] A. W. Zeng and B. Guo, "Characteristics of slow light in a magnetized plasma hyperbolic metamaterial waveguide," *Opt. Quantum Electron.*, vol. 49, no. 5, p. 200, May 2017, doi: 10.1007/s11082-017-1033-4.

[46] M.-J. Lee et al., "Experimental demonstration of spinor slow light," *Nature Commun.*, vol. 5, no. 1, p. 5542, Dec. 2014, doi: 10.1038/ncomms6542.

[47] A. Keshavarz and A. Zakery, "A novel terahertz semiconductor metamaterial for slow light device and dual-band modulator applications," *Plasmonics*, vol. 13, no. 2, pp. 459–466, 2018, doi: 10.1007/s11468-017-0531-3.

[48] S. Hu, H. Yang, S. Han, X. Huang, and B. Xiao, "Tailoring dual-band electromagnetically induced transparency in planar metamaterials," *J. Appl. Phys.*, vol. 117, no. 4, Jan. 2015, Art. no. 043107, doi: 10.1063/1.4906853.

[49] E. O. Polat and C. Kocabas, "Broadband optical modulators based on graphene supercapacitors," *Nano Lett.*, vol. 13, no. 12, pp. 5851–5857, Dec. 2013, doi: 10.1021/nl402616t.

[50] H. Cai et al., "All-optical and ultrafast tuning of terahertz plasmonic metasurfaces," *Adv. Opt. Mater.*, vol. 6, no. 14, Jul. 2018, Art. no. 1800143, doi: 10.1002/adom.201800143.

[51] L. Zhu et al., "Magnetic metamaterial analog of electromagnetically induced transparency and absorption," *J. Appl. Phys.*, vol. 117, no. 17, May 2015, Art. no. 17D146, doi: 10.1063/1.4916189.

[52] X. Zhang et al., "Electromagnetically induced absorption in a three-resonator metasurface system," *Sci. Rep.*, vol. 5, no. 1, p. 10737, Sep. 2015, doi: 10.1038/srep10737.

[53] J. He, P. Ding, J. Wang, C. Fan, and E. Liang, "Ultra-narrow band perfect absorbers based on plasmonic analog of electromagnetically induced absorption," *Opt. Exp.*, vol. 23, no. 5, p. 6083, Mar. 2015, doi: 10.1364/OE.23.006083.

[54] P. Tassin, L. Zhang, R. Zhao, A. Jain, T. Koschny, and C. M. Soukoulis, "Electromagnetically induced transparency and absorption in metamaterials: The radiating two-oscillator model and its experimental confirmation," *Phys. Rev. Lett.*, vol. 109, no. 18, Oct. 2012, Art. no. 187401, doi: 10.1103/PhysRevLett.109.187401.

[55] P. Bermel, A. Rodriguez, S. G. Johnson, J. D. Joannopoulos, and M. Soljačić, "Single-photon all-optical switching using waveguide-cavity quantum electrodynamics," *Phys. Rev. A, Gen. Phys.*, vol. 74, no. 4, Oct. 2006, Art. no. 043818, doi: 10.1103/PhysRevA.74.043818.

[56] G. Hétet, A. Peng, M. T. Johnsson, J. J. Hope, and P. K. Lam, "Characterization of electromagnetically-induced-transparency-based continuous-variable quantum memories," *Phys. Rev. A, Gen. Phys.*, vol. 77, no. 1, Jan. 2008, Art. no. 012323, doi: 10.1103/PhysRevA.77.012323.

[57] I. Novikova, R. L. Walsworth, and Y. Xiao, "Electromagnetically induced transparency-based slow and stored light in warm atoms," *Laser Photon. Rev.*, vol. 6, no. 3, pp. 333–353, May 2012, doi: 10.1002/lpor.201100021.

[58] C. L. Garrido Alzar, M. A. G. Martinez, and P. Nussenzveig, "Classical analog of electromagnetically induced transparency," *Amer. J. Phys.*, vol. 70, no. 1, pp. 37–41, Jan. 2002.

[59] D. Roy, "Two-photon scattering by a driven three-level emitter in a one-dimensional waveguide and electromagnetically induced transparency," *Phys. Rev. Lett.*, vol. 106, no. 5, Feb. 2011, Art. no. 053601, doi: 10.1103/PhysRevLett.106.053601.

[60] J. Harden, A. Joshi, and J. D. Serna, "Demonstration of double EIT using coupled harmonic oscillators and RLC circuits," *Eur. J. Phys.*, vol. 32, no. 2, pp. 541–558, Mar. 2011, doi: 10.1088/0143-0807/32/2/025.

[61] N. Xu, M. Manjappa, R. Singh, and W. Zhang, "Tailoring the electromagnetically induced transparency and absorbance in coupled Fano–Lorentzian metasurfaces: A classical analog of a four-level tripod quantum system," *Adv. Opt. Mater.*, vol. 4, no. 8, pp. 1179–1185, Aug. 2016, doi: 10.1002/adom.201600129.

[62] K. M. Devi, D. R. Chowdhury, G. Kumar, and A. K. Sarma, "Dual-band electromagnetically induced transparency effect in a concentrically coupled asymmetric terahertz metamaterial," *J. Appl. Phys.*, vol. 124, no. 6, Aug. 2018, Art. no. 063106, doi: 10.1063/1.5040734.

[63] F. Zhang, Q. Zhao, J. Zhou, and S. Wang, "Polarization and incidence insensitive dielectric electromagnetically induced transparency metamaterial," *Opt. Exp.*, vol. 21, no. 17, p. 19675, Aug. 2013, doi: 10.1364/OE.21.019675.

[64] H. Li et al., "Electromagnetically induced transparency with large delay-bandwidth product induced by magnetic resonance near field coupling to electric resonance," *Appl. Phys. Lett.*, vol. 106, no. 11, Mar. 2015, Art. no. 114101, doi: 10.1063/1.4915313.

[65] H. Li et al., "Low-loss metamaterial electromagnetically induced transparency based on electric toroidal dipolar response," *Appl. Phys. Lett.*, vol. 106, no. 8, Feb. 2015, Art. no. 083511, doi: 10.1063/1.4913888.

[66] H.-M. Li, S.-B. Liu, S.-Y. Liu, and H.-F. Zhang, "Electromagnetically induced transparency with large group index induced by simultaneously exciting the electric and the magnetic resonance," *Appl. Phys. Lett.*, vol. 105, no. 13, Sep. 2014, Art. no. 133514, doi: 10.1063/1.4897194.

[67] B. S. Tung, B. X. Khuyen, P. T. Linh, N. T. Tung, D. H. Manh, and V. D. Lam, "Polarization-insensitive electromagnetically-induced transparency in planar metamaterial based on coupling of ring and zigzag spiral resonators," *Mod. Phys. Lett. B*, vol. 34, no. 10, Apr. 2020, Art. no. 2050093, doi: 10.1142/S0217984920500931.

[68] X.-R. Jin et al., "Highly-dispersive transparency at optical frequencies in planar metamaterials based on two-bright-mode coupling," *Opt. Exp.*, vol. 19, no. 22, p. 21652, Oct. 2011, doi: 10.1364/OE.19.021652.

[69] S. Hayashi, D. V. Nesterenko, and Z. Sekkat, "Waveguide-coupled surface plasmon resonance sensor structures: Fano lineshape engineering for ultrahigh-resolution sensing," *J. Phys. D, Appl. Phys.*, vol. 48, no. 32, 2015, Art. no. 325303, doi: 10.1088/0022-3727/48/32/325303.

[70] L. Novotny, "Strong coupling, energy splitting, and level crossings: A classical perspective," *Amer. J. Phys.*, vol. 78, no. 11, pp. 1199–1202, Nov. 2010, doi: 10.1119/1.3471177.

[71] S. Zielińska-Raczyńska and D. Ziemkiewicz, "Frequency shifts of radiating particles moving in EIT metamaterial," *J. Opt. Soc. Amer. B, Opt. Phys.*, vol. 33, no. 3, p. 412, Mar. 2016, doi: 10.1364/JOSAB.33.000412.

[72] J. A. Souza, L. Cabral, R. R. Oliveira, and C. J. Villas-Boas, "Electromagnetically-induced-transparency-related phenomena and their mechanical analogs," *Phys. Rev. A, Gen. Phys.*, vol. 92, no. 2, Aug. 2015, Art. no. 023818, doi: 10.1103/PhysRevA.92.023818.

[73] E. H. El Boudouti, T. Mrabti, H. Al-Wahsh, B. Djafari-Rouhani, A. Akjouj, and L. Dobrzynski, "Transmission gaps and Fano resonances in an acoustic waveguide: Analytical model," *J. Phys., Condens. Matter*, vol. 20, no. 25, Jun. 2008, Art. no. 255212, doi: 10.1088/0953-8984/20/25/255212.

[74] M. Amin, A. Elayouch, M. Farhat, M. Addouche, A. Khelif, and H. Bağci, "Acoustically induced transparency using Fano resonant periodic arrays," *J. Appl. Phys.*, vol. 118, no. 16, Oct. 2015, Art. no. 164901, doi: 10.1063/1.4934247.

[75] G. Wang, L. Jin, P. Li, and Z. Xu, "Acoustically induced transparency by using concentric spherical shells with coaxial aperture array," *Appl. Phys. Lett.*, vol. 109, no. 7, Aug. 2016, Art. no. 073503, doi: 10.1063/1.4961504.

[76] M. Oudich et al., "Rayleigh waves in phononic crystal made of multilayered pillars: Confined modes, Fano resonances, and acoustically induced transparency," *Phys. Rev. A, Gen. Phys.*, vol. 9, no. 3, Mar. 2018, Art. no. 034013, doi: 10.1103/PhysRevApplied.9.034013.

[77] N. Papasimakis, V. A. Fedotov, N. I. Zheludev, and S. L. Prosvirnin, "Metamaterial analog of electromagnetically induced transparency," *Phys. Rev. Lett.*, vol. 101, no. 25, Dec. 2008, Art. no. 253903, doi: 10.1103/PhysRevLett.101.253903.

[78] L. Zhang, P. Tassin, T. Koschny, C. Kurter, S. M. Anlage, and C. M. Soukoulis, "Large group delay in a microwave metamaterial analog of electromagnetically induced transparency," *Appl. Phys. Lett.*, vol. 97, no. 24, Dec. 2010, Art. no. 241904, doi: 10.1063/1.3525925.

[79] Z. Xu, S. Li, Y. Liu, H. Zhao, and X. Yin, "Characteristic mode analysis of complex spoof localized surface plasmon resonators," *IEEE Access*, vol. 6, pp. 2871–2878, 2018, doi: 10.1109/ACCESS.2017.2785809.

[80] Z. Xu, X. Kong, J. Chang, D. F. Sievenpiper, and T. J. Cui, "Topological flat bands in self-complementary plasmonic metasurfaces," *Phys. Rev. Lett.*, vol. 129, no. 25, Dec. 2022, Art. no. 253001, doi: 10.1103/PhysRevLett.129.253001.

[81] X. Shen and T. J. Cui, "Ultrathin plasmonic metamaterial for spoof localized surface plasmons," *Laser Photon. Rev.*, vol. 8, no. 1, pp. 137–145, Jan. 2014, doi: 10.1002/lpor.201300144.

[82] P. A. Huidobro et al., "Magnetic localized surface plasmons," *Phys. Rev. X*, vol. 4, no. 2, Apr. 2014, Art. no. 021003, doi: 10.1103/PhysRevX.4.021003.

[83] Z. Xu, S. Liu, S. Li, and X. Yin, "Analog of electromagnetically induced transparency based on magnetic plasmonic artificial molecules with symmetric and antisymmetric states," *Phys. Rev. B, Condens. Matter*, vol. 99, no. 4, Jan. 2019, Art. no. 041104, doi: 10.1103/PhysRevB.99.041104.

[84] Z. Xu, J. Shi, R. J. Davis, X. Yin, and D. F. Sievenpiper, "Rainbow trapping with long oscillation lifetimes in gradient magnetoinductive metasurfaces," *Phys. Rev. A, Gen. Phys.*, vol. 12, no. 2, Aug. 2019, Art. no. 024043, doi: 10.1103/PhysRevApplied.12.024043.

[85] C.-K. Chen, Y.-C. Lai, Y.-H. Yang, C.-Y. Chen, and T.-J. Yen, "Inducing transparency with large magnetic response and group indices by hybrid dielectric metamaterials," *Opt. Exp.*, vol. 20, no. 7, p. 6952, Mar. 2012, doi: 10.1364/OE.20.006952.

[86] S. Jahani and Z. Jacob, "All-dielectric metamaterials," *Nature Nanotechnol.*, vol. 11, no. 1, pp. 23–36, Jan. 2016, doi: 10.1038/nnano.2015.304.

[87] Z. Xu, X. Cui, J. Shi, S. Liu, S. Li, and X. Yin, "Experimental demonstration of lattice-tailored scattering features of dielectric particle arrays at microwave frequencies," *Appl. Phys. Exp.*, vol. 12, no. 1, Jan. 2019, Art. no. 012006, doi: 10.7567/1882-0786/aaf5c3.

[88] F. Zhang et al., "Magnetically coupled electromagnetically induced transparency analogy of dielectric metamaterial," *Appl. Phys. Lett.*, vol. 104, no. 13, Mar. 2014, Art. no. 131907, doi: 10.1063/1.4870647.

[89] A. Kumar, M. Gupta, P. Pitchappa, Y. J. Tan, N. Wang, and R. Singh, "Topological sensor on a silicon chip," *Appl. Phys. Lett.*, vol. 121, no. 1, Jul. 2022, Art. no. 011101, doi: 10.1063/5.0097129.

[90] I. Al-Naib et al., "Excitation of a high-Q subradiant resonance mode in mirrored single-gap asymmetric split ring resonator terahertz metamaterials," *Appl. Phys. Lett.*, vol. 101, no. 7, Aug. 2012, Art. no. 071108, doi: 10.1063/1.4745790.

[91] X. Zhang et al., "Polarization-independent plasmon-induced transparency in a fourfold symmetric terahertz metamaterial," *IEEE J. Sel. Topics Quantum Electron.*, vol. 19, no. 1, Jan./Feb. 2013, Art. no. 8400707, doi: 10.1109/JSTQE.2012.2200656.

[92] Y. Xu, X. Wang, X. Chen, and L. Zhang, "Structure-based tunable metamaterials for electromagnetically induced transparency windows in low terahertz frequency," *J. Appl. Phys.*, vol. 127, no. 3, Jan. 2020, Art. no. 034501, doi: 10.1063/1.5140220.

[93] T. Ma, Q. Huang, H. He, Y. Zhao, X. Lin, and Y. Lu, "All-dielectric metamaterial analogue of electromagnetically induced transparency and its sensing application in terahertz range," *Opt. Exp.*, vol. 27, no. 12, p. 16624, Jun. 2019, doi: 10.1364/OE.27.016624.

[94] N. Liu et al., "Plasmonic analogue of electromagnetically induced transparency at the Drude damping limit," *Nature Mater.*, vol. 8, no. 9, pp. 758–762, Sep. 2009, doi: 10.1038/nmat2495.

[95] Y. Yang, I. I. Kravchenko, D. P. Briggs, and J. Valentine, "All-dielectric metasurface analogue of electromagnetically induced transparency," *Nature Commun.*, vol. 5, p. 5753, Dec. 2014, doi: 10.1038/ncomms6753.

[96] C. Wang et al., "Electromagnetically induced transparency at a chiral exceptional point," *Nature Phys.*, vol. 16, no. 3, pp. 334–340, Mar. 2020, doi: 10.1038/s41567-019-0746-7.

[97] L. J. Sherry, S.-H. Chang, G. C. Schatz, R. P. Van Duyne, B. J. Wiley, and Y. Xia, "Localized surface plasmon resonance spectroscopy of single silver nanocubes," *Nano Lett.*, vol. 5, no. 10, pp. 2034–2038, 2005, doi: 10.1021/nl0515753.

[98] F.-Y. Meng, Q. Wu, D. Erni, K. Wu, and J.-C. Lee, "Polarization-independent metamaterial analog of electromagnetically induced transparency for a refractive-index-based sensor," *IEEE Trans. Microw. Theory Techn.*, vol. 60, no. 10, pp. 3013–3022, Oct. 2012, doi: 10.1109/TMTT.2012.2209455.

[99] L. Zhu, J. H. Fu, F. Y. Meng, X. M. Ding, L. Dong, and Q. Wu, "Detuned magnetic dipoles induced transparency in microstrip line for sensing," *IEEE Trans. Magn.*, vol. 50, no. 1, pp. 1–4, Jan. 2014, doi: 10.1109/TMAG.2013.2279139.

[100] X. Yan, M. Yang, Z. Zhang, T. W. Wei, L. Liu, and J. Xie, "The terahertz electromagnetically induced transparency-like metamaterials for sensitive biosensors in the detection of cancer cells," *Biosensors Bioelectron.*, vol. 126, pp. 485–492, Feb. 2019, doi: 10.1016/j.bios.2018.11.014.

[101] J. Xu et al., "Terahertz microfluidic sensing with dual-torus toroidal metasurfaces," *Adv. Opt. Mater.*, vol. 9, no. 15, Aug. 2021, Art. no. 2100024, doi: 10.1002/adom.202100024.

[102] D. Rodrigo et al., "Mid-infrared plasmonic biosensing with graphene," *Science*, vol. 349, no. 6244, pp. 165–168, Jul. 2015, doi: 10.1126/science.aab2051.

[103] G. Soavi et al., "Broadband, electrically tunable third-harmonic generation in graphene," *Nature Nanotechnol.*, vol. 13, no. 7, pp. 583–588, Jul. 2018, doi: 10.1038/s41565-018-0145-8.

[104] H. Zhao, Y. Ren, L. Fang, and H. Lin, "Electromagnetic induced transparency in graphene waveguide structure for terahertz application," *Results Phys.*, vol. 16, Mar. 2020, Art. no. 102971, doi: 10.1016/j.rinp.2020.102971.

[105] X. He, P. Gao, and W. Shi, "A further comparison of graphene and thin metal layers for plasmonics," *Nanoscale*, vol. 8, no. 19, pp. 10388–10397, May 2016, doi: 10.1039/C5NR09061J.

[106] F. Pulizzi, O. Bubnova, S. Milana, D. Schilter, D. Abergel, and A. Moscatelli, "Graphene in the making," *Nature Nanotechnol.*, vol. 14, no. 10, pp. 914–918, Oct. 2019, doi: 10.1038/s41565-019-0552-5.

[107] J. Zhang, Z. Li, L. Shao, F. Xiao, and W. Zhu, "Active modulation of electromagnetically induced transparency analog in graphene-based microwave metamaterial," *Carbon*, vol. 183, pp. 850–857, Oct. 2021, doi: 10.1016/j.carbon.2021.07.069.

[108] W. Kong et al., "Path towards graphene commercialization from lab to market," *Nature Nanotechnol.*, vol. 14, no. 10, pp. 927–938, Oct. 2019, doi: 10.1038/s41565-019-0555-2.

[109] R. Ning, J. Bao, Y. Meng, and Z. Chen, "Wideband reciprocity tunable electromagnetically induced transparency in complementary graphene metasurface," *J. Opt.*, vol. 21, no. 4, Apr. 2019, Art. no. 045106, doi: 10.1088/2040-8986/ab0794.

[110] X. He et al., "Implementation of selective controlling electromagnetically induced transparency in terahertz graphene metamaterial," *Carbon*, vol. 123, pp. 668–675, Oct. 2017, doi: 10.1016/j.carbon.2017.08.016.

[111] B. Vasić, M. M. Jakovljević, G. Isić, and R. Gajić, "Tunable metamaterials based on split ring resonators and doped graphene," *Appl. Phys. Lett.*, vol. 103, no. 1, Jul. 2013, Art. no. 011102, doi: 10.1063/1.4812989.

[112] B. Xiao, S. Tong, A. Fyffe, and Z. Shi, "Tunable electromagnetically induced transparency based on graphene metamaterials," *Opt. Exp.*, vol. 28, no. 3, p. 4048, Feb. 2020, doi: 10.1364/OE.382485.

[113] C. Zhang et al., "Anisotropic nonlinear optical properties of a SnSe flake and a novel perspective for the application of all-optical switching," *Adv. Opt. Mater.*, vol. 7, no. 18, Sep. 2019, Art. no. 1900631, doi: 10.1002/adom.201900631.

[114] Y. K. Srivastava et al., "MoS_2 for ultrafast all-optical switching and modulation of THz Fano metaphotonic devices," *Adv. Opt. Mater.*, vol. 5, no. 23, Dec. 2017, Art. no. 1700762, doi: 10.1002/adom.201700762.

[115] W. J. Padilla, A. J. Taylor, C. Highstrete, M. Lee, and R. D. Averitt, "Dynamical electric and magnetic metamaterial response at terahertz frequencies," *Phys. Rev. Lett.*, vol. 96, Mar. 2006, Art. no. 107401, doi: 10.1103/PhysRevLett.96.107401.

[116] M. Manjappa, A. Solanki, A. Kumar, T. C. Sum, and R. Singh, "Solution-processed lead iodide for ultrafast all-optical switching of terahertz photonic devices," *Adv. Mater.*, vol. 31, no. 22, Aug. 2019, Art. no. 1901455, doi: 10.1002/adma.201901455.

[117] N.-H. Shen et al., "Optically implemented broadband blueshift switch in the terahertz regime," *Phys. Rev. Lett.*, vol. 106, no. 3, Jan. 2011, Art. no. 037403, doi: 10.1103/PhysRevLett.106.037403.

[118] X. Zhao et al., "Optically modulated ultra-broadband all-silicon metamaterial terahertz absorbers," *ACS Photon.*, vol. 6, no. 4, pp. 830–837, Apr. 2019, doi: 10.1021/acsphotonics.8b01644.

[119] Y. Hu et al., "Ultrafast terahertz frequency and phase tuning by all-optical molecularization of metasurfaces," *Adv. Opt. Mater.*, vol. 7, no. 22, Nov. 2019, Art. no. 1901050, doi: 10.1002/adom.201901050.

[120] K. Fan et al., "Optically tunable terahertz metamaterials on highly flexible substrates," *IEEE Trans. Terahertz Sci. Technol.*, vol. 3, no. 6, pp. 702–708, Nov. 2013, doi: 10.1109/TTHZ.2013.2285619.

[121] M. R. Shcherbakov et al., "Ultrafast all-optical tuning of direct-gap semiconductor metasurfaces," *Nature Commun.*, vol. 8, no. 1, p. 17, Dec. 2017, doi: 10.1038/s41467-017-00019-3.

[122] M. Manjappa, Y. K. Srivastava, L. Cong, I. Al-Naib, and R. Singh, "Active photoswitching of sharp Fano resonances in THz metadevices," *Adv. Mater.*, vol. 29, no. 3, Jan. 2017, Art. no. 1603355, doi: 10.1002/adma.201603355.

[123] T.-T. Yeh, H. Shirai, C.-M. Tu, T. Fuji, T. Kobayashi, and C.-W. Luo, "Ultrafast carrier dynamics in Ge by ultra-broadband mid-infrared probe spectroscopy," *Sci. Rep.*, vol. 7, no. 1, p. 40492, Jan. 2017, doi: 10.1038/srep40492.

[124] J. Zhou et al., "Controllable all-optical modulation speed in hybrid silicon-germanium devices utilizing the electromagnetically induced transparency effect," *Nanophotonics*, vol. 9, no. 9, pp. 2797–2807, Jul. 2020, doi: 10.1515/nanoph-2020-0017.

[125] H. Liu, G. Ren, Y. Gao, Y. Lian, Y. Qi, and S. Jian, "Tunable subwavelength terahertz plasmon-induced transparency in the InSb slot waveguide side-coupled with two stub resonators," *Appl. Opt.*, vol. 54, no. 13, p. 3918, May 2015, doi: 10.1364/AO.54.003918.

[126] J. A. Sánchez-Gil and J. G. Rivas, "Thermal switching of the scattering coefficients of terahertz surface plasmon polaritons impinging on a finite array of subwavelength grooves on semiconductor surfaces," *Phys. Rev. B, Condens. Matter*, vol. 73, no. 20, May 2006, Art. no. 205410, doi: 10.1103/PhysRevB.73.205410.

[127] M. Oszwałdowski and M. Zimpel, "Temperature dependence of intrinsic carrier concentration and density of states effective mass of heavy holes in InSb," *J. Phys. Chem. Solids*, vol. 49, pp. 1179–1185, Aug. 1988, doi: 10.1016/0022-3697(88)90173-4.

[128] S. Ghafari, M. R. Forouzeshfard, and Z. Vafapour, "Thermo optical switching and sensing applications of an infrared metamaterial," *IEEE Sensors J.*, vol. 20, no. 6, pp. 3235–3241, Mar. 2020, doi: 10.1109/JSEN.2019.2955672.

[129] K. Hoffmann and Z. Skvor, "Active resonator," in *Proc. Int. Conf. Trends Communications. Tech. Program (EUROCON)*, Bratislava, Slovakia, vol. 1, Jul. 2001, pp. 164–166, doi: 10.1109/EURCON.2001.937789.

[130] Y. Fan et al., "An electromagnetic modulator based on electrically controllable metamaterial analogue to electromagnetically induced transparency," *Sci. Rep.*, vol. 7, no. 1, p. 40441, Mar. 2017, doi: 10.1038/srep40441.

[131] R. Yang et al., "Active control of EIT-like response in a symmetry-broken metasurface with orthogonal electric dipolar resonators," *Photon. Res.*, vol. 7, no. 9, p. 955, Sep. 2019, doi: 10.1364/PRJ.7.000955.

[132] T. H. Feng and H. P. Han, "Tunable transmission-line metamaterials mimicking electromagnetically induced transparency," *J. Electron. Mater.*, vol. 45, no. 11, pp. 6038–6042, Nov. 2016, doi: 10.1007/s11664-016-4807-8.

[133] P. Pitchappa et al., "Active control of near-field coupling in conductively coupled microelectromechanical system metamaterial devices," *Appl. Phys. Lett.*, vol. 108, no. 11, Mar. 2016, Art. no. 111102, doi: 10.1063/1.4943974.

[134] Y. Huang, K. Nakamura, Y. Takida, H. Minamide, K. Hane, and Y. Kanamori, "Actively tunable THz filter based on an electromagnetically induced transparency analog hybridized with a MEMS metamaterial," *Sci. Rep.*, vol. 10, no. 1, p. 20807, Nov. 2020, doi: 10.1038/s41598-020-77922-1.

[135] X. J. He et al., "Dynamic manipulation of electromagnetically induced transparency with MEMS metamaterials," *Integr. Ferroelectr.*, vol. 161, no. 1, pp. 85–91, Mar. 2015, doi: 10.1080/10584587.2015.1036636.

[136] P. Pitchappa, M. Manjappa, C. P. Ho, R. Singh, N. Singh, and C. Lee, "Active control of electromagnetically induced transparency analog in terahertz MEMS metamaterial," *Adv. Opt. Mater.*, vol. 4, no. 4, pp. 541–547, Apr. 2016, doi: 10.1002/adom.201500676.

[137] L. Zhu and L. Dong, "Electromagnetically induced transparency metamaterials: Theories, designs and applications," *J. Phys. D, Appl. Phys.*, vol. 55, no. 26, Jun. 2022, Art. no. 263003, doi: 10.1088/1361-6463/ac60cc.

[138] L. Cong, Y. K. Srivastava, A. Solanki, T. C. Sum, and R. Singh, "Perovskite as a platform for active flexible metaphotonic devices," *ACS Photon.*, vol. 4, no. 7, pp. 1595–1601, 2017.

[139] T. Zhang et al., "Machine learning and evolutionary algorithm studies of graphene metamaterials for optimized plasmon-induced transparency," *Opt. Exp.*, vol. 28, no. 13, p. 18899, Jun. 2020, doi: 10.1364/OE.389231.

[140] L. Lu, J. D. Joannopoulos, and M. Soljačić, "Topological photonics," *Nature Photon.*, vol. 8, no. 11, pp. 821–829, Oct. 2014, doi: 10.1038/nphoton.2014.248.

[141] A. Kumar et al., "Phototunable chip-scale topological photonics: 160 Gbps waveguide and demultiplexer for THz 6G communication," *Nature Commun.*, vol. 13, no. 1, p. 5404, Sep. 2022, doi: 10.1038/s41467-022-32909-6.

[142] C. Marques et al., "Fast Bragg grating inscription in PMMA polymer optical fibres: Impact of thermal pre-treatment of preforms," *Sensors*, vol. 17, no. 4, p. 891, Apr. 2017, doi: 10.3390/s17040891.

[143] V. S. Chaudhary, D. Kumar, B. P. Pandey, and S. Kumar, "Advances in photonic crystal fiber-based sensor for detection of physical and biochemical parameters—A review," *IEEE Sensors J.*, vol. 23, no. 2, pp. 1012–1023, Jan. 2023, doi: 10.1109/JSEN.2022.3222969.

[144] V. Kumar, S. K. Raghuwanshi, and S. Kumar, "Recent advances in carbon nanomaterials based SPR sensor for biomolecules and gas detection—A review," *IEEE Sensors J.*, vol. 22, no. 16, pp. 15661–15672, Aug. 2022, doi: 10.1109/JSEN.2022.3191042.

[145] A. Shadab, S. K. Raghuwanshi, and S. Kumar, "Advances in microfabricated fiber Bragg grating for detection of physical, chemical, and biological parameters—A review," *IEEE Sensors J.*, vol. 22, no. 16, pp. 15650–15660, Aug. 2022, doi: 10.1109/JSEN.2022.3188813.

Zhixia Xu (Member, IEEE) was born in Wuxi, China. He received the B.Eng. degree in electronic information science and technology from Dalian Maritime University, Dalian, China, in 2015, and the Ph.D. degree in electromagnetic field and microwave technique from Southeast University, Nanjing, China, in 2019.

From 2018 to 2019, he worked as a Visiting Graduate Student at the University of California at San Diego, La Jolla, CA, USA. He is currently an Associate Professor with Dalian Maritime University. He also holds a postdoctoral position at the State Key Laboratory of Millimeter Waves, Southeast University. His current research interests include periodic structures, photonic topological insulators, sensors, and antennas.

Yi Wang received the B.Eng. degree in communication engineering from Dalian Maritime University (DMU), Dalian, Liaoning, China, in 2020, where he is currently pursuing the M.Eng. degree in information and communication engineering.

His current research interests include electromagnetically induced transparency (EIT)-like metamaterials in sensing applications.

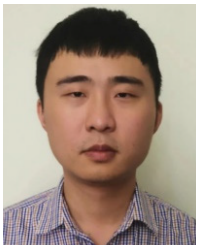

Siyuan Liu (Graduate Student Member, IEEE) received the Ph.D. degree in engineering from the School of Information Science and Engineering, Southeast University, Nanjing, China, in December 2022.

He also has published many high-level papers and participated in many national, provincial, and ministerial projects. He has been engaged in the research of electromagnetic metamaterials, electromagnetic parameter sensors, and analog electromagnetically induced transparency for a long time.

Jitong Ma received the B.S. degree in electronic information engineering from Hohai University, Nanjing, China, in 2013, and the M.S. degree and the Ph.D. degree in signal and information processing from the Dalian University of Technology, Dalian, China, in 2015 and 2020, respectively.

From 2018 to 2019, he was a Joint Supervision Ph.D. Student with the Department of Electrical and Computer Engineering, North Carolina State University, Raleigh, NC, USA. He is currently a Lecturer with the Information Science and Technology College, Dalian Maritime University, Dalian. His research interests include wireless communication and statistical signal processing.

Shaojun Fang received the Ph.D. degree in communication and information systems from Dalian Maritime University (DMU), Dalian, Liaoning, China, in 2001.

Since 1982, he has been with DMU, where he is currently the Head Professor with the School of Information Science and Technology. He has authored or coauthored three books and over 100 journal articles and conference papers. His recent research interests include passive RF components, patch antennas, and computational electromagnetics.

Dr. Fang was a recipient of the Best Doctor's Dissertation Award of Liaoning Province in 2002 and the Outstanding Teacher Award of the Ministry of Transport of China.

Haotian Wu was born in Xi'an, China, in 1992. He received the B.E. degree in electrical and information engineering from Central South University, Changsha, China, in 2014, and the Ph.D. degree in electromagnetic field and microwave technology from Southeast University, Nanjing, China, in 2020.

He is currently working as a Postdoctoral Research Fellow at the Nanophononics Laboratory, Nanyang Technological University, Singapore. His current research interests include electromagnetic theory, metamaterials, metasurfaces, and topological insulators.